Chem Soc Rev

REVIEW ARTICLE

View Article Online
View Journal | View Issue

Cite this: *Chem. Soc. Rev.*, 2020, **49**, 4926

Semi-biological approaches to solar-to-chemical conversion

Xin Fang, Shafeer Kalathil and Erwin Reisner *

This review presents a comprehensive summary of the recent development in semi-artificial photosynthesis, a biological-material hybrid approach to solar-to-chemical conversion that provides new concepts to shape a sustainable future fuelled by solar energy. We begin with a brief introduction to natural and artificial photosynthesis, followed by a discussion of the motivation and rationale behind semi-artificial photosynthesis. Then, we summarise how various enzymes can be combined with synthetic materials for light-driven water oxidation, H_2 evolution, CO_2 reduction, and chemical synthesis more broadly. In the following section, we discuss the strategies to incorporate microorganisms in photocatalytic and (photo)electrochemical systems to produce fuels and chemicals with renewable sources. Finally, we outline emerging analytical techniques to study the bio-material hybrid systems and propose unexplored research opportunities in the field of semi-artificial photosynthesis.

Received 28th October 2019

DOI: 10.1039/c9cs00496c

rsc.li/chem-soc-rev

1 Introduction

The consequences of anthropogenic carbon emissions call for innovative strategies to develop renewable energy technologies. Photovoltaics (PV) is the leading technology for solar energy conversion,[1,2] but it shows disadvantages in intermittency and long-distance electricity transmission. Artificial photosynthesis is a process that converts solar energy into fuels and it thereby circumvents these drawbacks by storing solar energy in chemical bonds using synthetic light absorbers and catalysts.[3,4] While synthetic catalysts still encounter challenges in solar-to-chemical conversion, nature provides evolutionarily-optimised biocatalysts. This review summarises how this biological machinery can be leveraged to catalyse light-driven reactions by an emerging technology termed "semi-artificial photosynthesis", in which biocatalysts in the form of enzymes or microorganisms are incorporated with particles or structurally-crafted electrodes to produce fuels or chemicals.

Department of Chemistry, University of Cambridge, Lensfield Road, Cambridge CB2 1EW, UK. E-mail: reisner@ch.cam.ac.uk

1.1 Natural photosynthesis

Photosynthesis occurs in photoautotrophs such as cyanobacteria, algae and higher plants, which harvest solar energy to produce biomass and O_2 from CO_2 and H_2O. Photosynthesis is accomplished

Xin Fang

Xin Fang obtained his PhD degree from the University of Cambridge under the supervision of Prof. Erwin Reisner. His doctoral research focused on establishing efficient solar-to-chemical conversion avenues with biocatalysts in the form of enzymes and whole cells. His research broadly traverses the fields of biocatalysis, materials science, electrochemistry, and photocatalysis, with the aim to shift the paradigm of artificial photosynthesis by rationally integrating biocatalysts with synthetic components. Before that, he studied at Fudan University and Sichuan University for a Master and Bachelor's degree in polymer science, respectively.

Shafeer Kalathil

Shafeer Kalathil obtained his PhD in Chemical Engineering at Yeungnam University under the supervision of Prof. Moo Hwan Cho, where he worked on microbial fuel cells and microbial cell factories. He was a JSPS Fellow at the University of Tokyo (with Prof. Kazuhito Hashimoto) and a Postdoctoral Fellow at KAUST (with Prof. Pascal Saikaly). He joined the group of Prof. Erwin Reisner (University of Cambridge) as a Marie Curie Fellow to work on the microbial electrosynthesis of value-added products from waste-carbon. His current research focuses on the integration of light-harvesting materials with microbes to produce industrially relevant chemicals from carbon dioxide.

by two phases of reactions: the light reaction uses solar energy to generate the energy carrier adenosine triphosphate (ATP) and the reduced nicotinamide adenine dinucleotide phosphate (NADPH) as the reducing agent; the dark reaction then uses the ATP and NADPH to reduce atmospheric CO_2 into carbohydrates through the Calvin cycle.[5]

1.1.1 Light reactions. The light reaction is carried out in the thylakoid membrane by the photosynthetic apparatus, including photosystem II (PSII) and photosystem I (PSI), cytochrome b_6f (cyt b_6f), the plastoquinone (PQ) pool, plastocyanin (PC), ferredoxin (Fd), ferredoxin–$NADP^+$ reductase (FNR) and ATP synthase (ATPase) (Fig. 1a).[6] The two light absorbing photosystems both contain antenna complexes and reaction centres. The antenna complex comprises hundreds of pigments (chlorophylls and carotenoids), which capture photons and funnel the light energy to the reaction centre at a high quantum efficiency of $>95\%$. The reaction centre is a transmembrane protein–pigment complex, where electrons are excited and transferred to the downstream chemical synthesis pathway. The reaction centre chlorophylls in PSII and PSI are referred to as P680 and P700, respectively. The two photosystems function in concert to efficiently transfer electrons from H_2O to $NADP^+$ through a "Z-scheme" (Fig. 1b). The electron transfer in the thylakoid membrane is initiated by PSII, which absorbs photons and extracts electrons from H_2O to reduce its terminal electron acceptor, plastoquinone B (Q_B). The fully reduced plastohydroquinone (Q_BH_2) dissociates from the reaction centre and transfers its electrons to cyt b_6f, which forwards the electrons to PSI *via* a small copper-containing protein PC. At PSI, the arriving electrons are energised by a second excitation and finally delivered to FNR to reduce $NADP^+$ to NADPH (Fig. 1a).[5] Simultaneously, the water oxidation and the electron transport induce proton translocation from the stroma to the lumen, which generates a proton gradient and chemiosmosis driving the synthesis of ATP by ATPase.

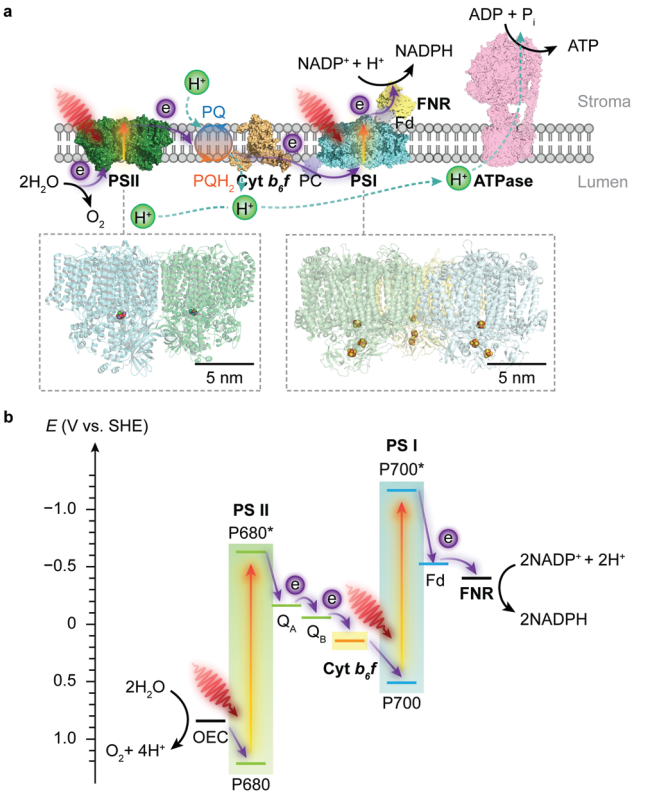

Fig. 1 Schematic illustration of the light reaction in natural photosynthesis. (a) Electron and proton transfer pathways in the thylakoid membrane. At the start of the photosynthetic chain is PSII that oxidises H_2O and releases O_2 and protons upon light absorption. The electrons are then delivered to PSI *via* a plastoquinone (PQ) pool, cyt b_6f and plastocyanin (PC). Electrons are photoexcited for a second time at PSI to reduce $NADP^+$ to NADPH *via* a ferredoxin (Fd) and a ferredoxin–$NADP^+$ reductase (FNR). The water oxidation and electron transport also induce proton translocation from the stroma to the lumen, which generates a proton gradient and chemiosmosis driving the synthesis of ATP by ATP synthase (ATPase). Protein data bank ID: PSII (4ub6), cyt b_6f (4h44), PC (1bxu), PSI (5oy0), Fd-FNR (2yvj), ATPase (6fkf). (b) Energy level diagram of the Z-scheme electron transfer in the thylakoid membrane. The redox carriers are placed at their midpoint redox potentials at pH 7.0.

Erwin Reisner

Erwin Reisner received his PhD degree from the University of Vienna (with Prof. Bernhard K. Keppler), and postdoctoral training at the Massachusetts Institute of Technology (with Prof. Stephen J. Lippard) and the University of Oxford (with Prof. Fraser A. Armstrong) in biological inorganic chemistry, before moving to the University of Cambridge where he is currently the Professor of Energy and Sustainability. His laboratory explores the interface of chemical biology, synthetic chemistry, materials science and engineering relevant to the development of solar-driven processes for the sustainable synthesis of fuels and chemicals.

1.1.2 Dark reactions. The NADPH and ATP produced by the light reaction are then used to reduce CO_2 to carbohydrates in the Calvin cycle. During the process, CO_2 and H_2O are combined with the carbon acceptor ribulose-1,5-bisphosphate to yield two molecules of 3-phosphoglycerate. This intermediate is then reduced to glyceraldehyde-3-phosphate with ATP and NADPH. The cycle closes with the regeneration of ribulose-1,5-bisphosphate, the initial CO_2 acceptor.[6] The Calvin cycle accounts for more than 90% of carbon assimilation on earth. Central to this reaction is ribulose-1,5-bisphosphate carboxylase/oxygenase (Rubisco) that covalently fixes CO_2 to a carbon skeleton.[7,8] Rubisco is abundant in nature and operates using atmospheric CO_2 concentrations ($\sim$415 ppm). However, it also displays slow catalysis and low selectivity. The turnover frequency (TOF) of Rubisco is typically less than 10 s^{-1}, rendering the photosynthetic CO_2 fixation inefficient under optimal conditions.[8] It also confuses the substrate (CO_2) and the product (O_2) of photosynthesis,

which offsets the CO_2 uptake and saddles oxygenic phototrophs with energy-dissipating photorespiration.[9]

Photorespiration can consume 25% of carbon photosynthetically fixed by C_3 plants and this carbon loss is more severe at higher temperature. Some tropical plants, namely C_4 plants, overcome the disadvantageous photorespiration by deploying an additional C_4 pathway to increase the local concentration of CO_2. In these plants, phosphoenolpyruvate is first carboxylated into a four-carbon compound oxaloacetate, which undergoes further transformations and decarboxylation to release CO_2. The released CO_2 is then scavenged by Rubisco and drawn into the Calvin cycle with minimal photorespiration.[6]

1.1.3 Photosynthetic efficiency. Photosynthetic organisms have evolved highly efficient light-harvesting systems with a quantum efficiency of more than 90%. Nevertheless, the overall photosynthetic efficiency is low: the highest efficiency measured under field conditions is 2.9% for C_3 and 4.2% for C_4 plants and typical efficiencies are 0.2–1% for crop plants.[10,11] Several reasons are responsible for the low photosynthetic efficiency:[10,12] (1) As the pigments in photosystems and antennae are primarily sensitive to visible light (λ = 400–700 nm), photosystems can only intercept 48.7% of the incident solar energy; (2) light reflection and transmission due to weak absorption of green light (λ = 500–600 nm) cause at least 4.9% of energy loss;[13] (3) 6.6% of energy will be dissipated as heat during the transfer in antenna complexes, before reaching the red light-absorbing chlorophylls in the reaction centres; (4) energy expenditure associated with carbohydrate synthesis accounts for 24.6% and 28.7% for C_3 and C_4 plants, respectively; (5) oxygenation and ensuing photorespiration cost extra 6.1% of energy in C_3 plants; (6) respiratory metabolism for maintenance and growth consumes a minimum of 1.9% (C_3 plants) and 2.5% (C_4 plants) of the entire energy input from solar irradiation. Summing all of these energy losses, the maximal theoretical solar-to-biomass conversion efficiencies are 4.6% for C_3 plants and 6.0% for C_4 plants (30 °C).[10,12]

1.1.4 Photobiological H_2 production and N_2 fixation. Cyanobacteria and microalgae contain thylakoid membranes to carry out photosynthetic reactions,[14] and they can produce H_2 in anaerobic conditions by partially diverting photo-generated electrons from PSI towards H_2-producing hydrogenases (H_2ases).[15–17] However, inhibition of H_2ase by evolved O_2 renders this process transient and economically unfeasible. In addition, electron transport from PSI to H_2ase requires diffusional electron carriers such as ferredoxins, which impose a kinetic limit on the overall process.[18]

Some cyanobacteria can also fix atmospheric N_2 using solar energy when nitrogen-containing substrates (NH_3, NO_3^-, *etc.*) are not available.[19,20] However, nitrogenase (N_2ase), the enzyme responsible for N_2 fixation, is sensitive to oxygen.[21] Therefore, cyanobacteria have developed strategies to separate the oxygenic photosynthesis and N_2 fixation spatially (in different cells) or temporally (during the night) to protect the N_2ase from irreversible damage.[20]

1.2 Artificial photosynthesis

Artificial photosynthesis does not reproduce the exact reactions occurring in photoautotrophs, but exploits light absorbers and catalysts to produce fuels and chemicals with earth-abundant feedstock chemicals such as H_2O and CO_2. A prototype reaction is light-driven water splitting, which produces H_2 as a suitable energy carrier to overcome the intermittency of solar irradiation.[22,23] Solar water splitting has been under intense investigation over several decades, but it still faces challenges arising from solar light harvesting, catalyst stability, interfacial charge transfer and the water oxidation reaction.[24] The four-electron water oxidation to oxygen involves multiple bond rearrangements and concerted proton release, and thus causes both a thermodynamic barrier and kinetic sluggishness that confront the existing catalytic chemistry.[25]

Thermodynamics determines the suitability of light absorbers from an energetic perspective (Fig. 2), as illustrated by the water splitting reaction, where the energy band positions should straddle the electrochemical potentials of the half reactions, *i.e.*, hydrogen evolution reaction (HER) and oxygen evolution reaction (OER) (Fig. 3a). The band gap of the light absorbers should not be too wide to enable the visible light (400–800 nm, band gap: 1.53–3.10 eV) utilisation.[26] The thermodynamic redox potentials of light absorbers should also be properly aligned with respect to their energy band positions to prevent themselves from photo-induced corrosion.[27]

Several semiconductors whose electronic structures suffice in theory for overall water splitting with visible light have been under investigation, such as C_3N_4, CdS and $Y_2Ti_2O_5S_2$.[22] An alternative strategy is to align the band position of two light absorbers and catalyse HER and OER with the aid of electron mediators (Fig. 3b),[22,28] which resembles the photosynthetic electron transfer (''Z-scheme'') in the thylakoid membrane (Fig. 1b). This two-step excitation system can expand the light absorption by harvesting lower-energy photons,[22,29] and can bring together materials that can only drive either HER or OER alone.[30–32] Such tandem systems enable larger driving forces for water splitting, and permit higher theoretical solar-to-hydrogen conversion efficiencies than the single light-absorber systems.[33] Yet two light absorbers also multiply chances of charge recombination and pose challenges to balance the electron transfer kinetics of the half reactions.[3,22]

The implementation of artificial photosynthesis is often envisioned in two forms: first, light absorbers are loaded with electrocatalysts and then suspended in a photoreactor (Fig. 3c).[34] Second, solar fuel synthesis is performed in a photoelectrochemical (PEC) cell, where catalysts are immobilised on photoelectrodes and photoinduced electrons flow across the external circuit (Fig. 3d).[35] From a techno-economical viewpoint, the photocatalytic system may be more advantageous, as PEC systems may be required to achieve up to ~25% solar-to-hydrogen (STH) conversion efficiency to rival with petrol in energy prices, primarily due to higher investment in installations, whereas a STH efficiency of 5–10% would possibly suffice to render photocatalytic reactors cost-competitive.[4,34] However, the highest STH conversion efficiency of particle-based systems is around 1%,[28] whereas that of electrode-based systems can typically achieve more than 10%.[36,37] PEC systems also have several merits that are appealing for fundamental research and practical applications: (1) immobilisation of photocatalysts on electrodes enables in-depth studies of half-reactions

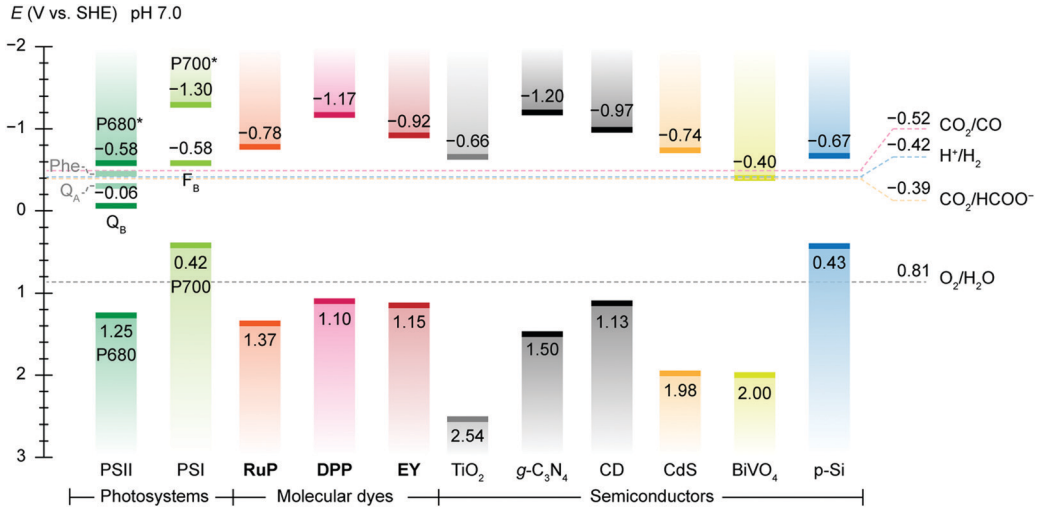

Fig. 2 Energy band edges of light absorbers used in semi-artificial photosynthesis. The band edge locations of photosystems are represented by redox potentials of their reaction centre chlorophylls, *i.e.* P680 (PSII) and P700 (PSI) and terminal electron acceptors, *i.e.*, Q_B (PSII) and a [Fe–S] cluster F_B (PSI).[119] For molecular dyes, the lowest unoccupied molecular orbital (LUMO) and the highest occupied molecular orbital (HOMO) are used as conceptual equivalents of conduction band edge and valence band edge in semiconductors. Data source: **DPP**,[147] **RuP**,[147] **Eosin Y** (**EY**),[292] TiO_2,[293] g-C_3N_4,[294] carbon dot (CD),[283,295] CdS,[296] $BiVO_4$,[157] p-Si.[162] The redox potentials CO_2/CO (catalysed by CODH),[186] H^+/H_2 (catalysed by H_2ase),[133] CO_2/$HCOO^-$ (catalysed by FDH),[183] and O_2/H_2O are displayed as references. The energy band edges and redox potentials are corrected with respect to SHE at pH 7.0 *via* the Nernstian relationship (25 °C).

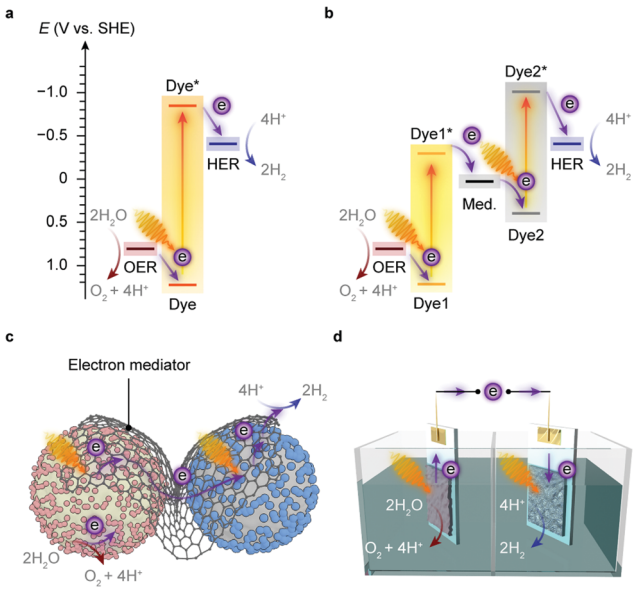

Fig. 3 Artificial approaches to solar-to-chemical conversion. (a and b) Energy level diagrams of light-driven water splitting at pH 7.0: single-step excitation (a) and two-step excitation (b). Dye and Dye*: the light absorber in the ground and excited state, respectively. Med.: redox mediator. (c) Representation of a two-step photocatalytic water-splitting system with semiconductor particles and HER and OER co-catalysts. The HER and OER photocatalysts are interfaced with a solid-state electron mediator. (d) Representation of a PEC tandem water-splitting system.

individually without sacrificial reagents and allows for *in situ* probing of photoredox chemistry through spectroscopic methodologies;[38–40] (2) from an application's perspective, the electrode-based configuration enables separation of H_2 and O_2 in a two-compartment configuration,[41] and can be transformed into a continuous fuel-production system with a flowing electrolyte solution.[42] On the other side, drawbacks emerge: (1) the preparation of photoelectrodes requires conductivity and high film-forming capability of semiconductors; (2) the operation of a PEC cell can generate pH gradients and cause mass transfer limitations that account for substantial potential loss and subject electrodes to increasingly corrosive environments;[43,44] (3) the internal resistance often necessitates external bias voltages to drive the electron flow from a photoanode to a photocathode.

Sustainable transformation of CO_2 to chemicals and fuels would provide a means to close the loop of the anthropogenic carbon cycle and offer a viable solution for carbon capture and utilisation.[45] The linear CO_2 molecule is chemically stable, and thus activating the C=O bond for the ensuing endothermic reactions may incur a substantial energy penalty, which is reflected in the negative potential (−1.9 V *vs.* SHE, pH 7.0) for the one-electron reduction to $CO_2^{\bullet-}$.[46–48] Although such a high energy barrier can be overcome by large electrochemical potentials or high temperature, it results in poor energetic efficiencies for subsequent fuel synthesis. The activation of CO_2 is followed by a stepwise proton and/or electron transfer, which gives rise to furcate reaction pathways towards miscellaneous products.[45,49] In addition, due to the low solubility of CO_2 in water (0.033 mol L^{-1} at 25 °C, 100 kPa),[46] the reduction of CO_2 usually competes with H_2 evolution from H_2O, which further reduces the selectivity and the conversion efficiency.[48] Current photocatalytic CO_2 reduction systems can produce CO and formate, but still struggle to produce multicarbon chemicals such as ethylene and ethanol selectively, which challenges the economic exploitation of this approach.[50]

Artificial photosynthesis has recently been extended to drive reactions such as N_2 reduction. Today, industrial N_2 reduction

relies on the energy-demanding Haber–Bosch process that requires H_2, high temperature (300–500 °C) and high pressure (150–200 atm).[51,52] The Haber–Bosch process also entails considerable CO_2 emission during the production of the inlet H_2 from natural gas (1.87 kg CO_2 per 1 kg NH_3).[51] The intense energy consumption and environmental stress arising from the Haber–Bosch process have spurred explorations in sustainable routes for N_2-to-NH_3 transformation. Photocatalytic N_2 reduction uses solar light to replace fossil fuels as the energy source and water instead of natural gas as the hydrogen source and operates at room temperature and atmospheric pressure.[53–56] The prospect of this approach largely depends on the photocatalysts that generate photoelectrons to reduce the stable and inert N≡N bond. However, the existing photocatalytic N_2 reduction systems still display low solar-to-chemical conversion efficiencies (typically below 0.02%),[51,55,57] and current studies encounter technical difficulties in reliable NH_3 quantification and elimination of probable experimental artefacts.[58]

2 Semi-artificial photosynthesis

Artificial photosynthesis establishes solar-to-fuel pathways to address the global energy challenge, but the bottlenecks are key-step reactions during the fuel-forming process, such as water oxidation and selective CO_2 activation. Biology is highly capable of tackling these synthetic challenges through the naturally-refined biocatalytic machinery. Enzymes comprise only a handful of earth-abundant metal atoms as catalytic centres and cofactors, which are embedded in polypeptide chains (Fig. 4a).[46] Enzymes perfectly orchestrate the electron and proton transfer, reactant delivery, bond rearrangement and product removal at the active site, thereby reducing the energy threshold and accelerating the reaction kinetics. Enzymes widely employ steric hindrance and electrostatic or hydrogen bond interactions to stabilise selected intermediates and transition states, and therefore provide an efficient reaction path towards a single product.[59] The catalytic prowess of enzymes has inspired synthetic endeavours to mimic their active sites and ligand environments, and to exploit the biological strategies to stabilise intermediates and control selectivity.[60–62] Although synthetic mimics are making progress, they have not yet reproduced the performance of their natural models in terms of catalytic rate, selectivity and electrochemical overpotentials under benign aqueous conditions.

Microorganisms can produce complex multicarbon compounds from simple feedstocks through their intracellular pathways (Fig. 4b). They can also maintain metabolic homeostasis at varying environmental and nutritional conditions. The enzymatic machinery embedded in its well-controlled and confined native environment benefits from the innate regulation mechanisms and can be repaired and regenerated when necessary. On the other side, microorganisms rank their physiological needs to survive ahead of synthetic efficiency to produce target chemicals. Carbon and electron fluxes in the metabolism are partially directed towards biomass synthesis for cell growth and maintenance, which reduces the

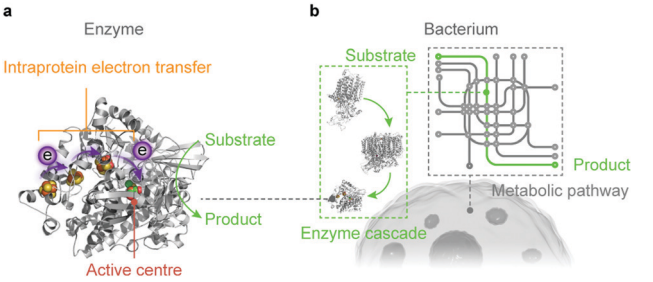

Fig. 4 Biocatalysts in the form of an enzyme (a) and a bacterium (b) used in semi-artificial photosynthesis.

pathway efficiency in chemical synthesis. Moreover, rerouting biochemical pathways towards desired products encounters resistance from the intracellular regulation, which renders such alteration problematic.[63,64]

Artificial photosynthesis, however, permits more flexibility in system design and modification. Taking light harvesting as an example: most chlorophylls in nature have a minimum absorption to green light (λ = 500–600 nm),[13] which partially accounts for the low photosynthetic efficiency, whereas in artificial photosynthesis, broadband absorption can be readily achieved with a variety of semiconductors and molecular dyes.[11] Furthermore, artificial systems allow for coupling fuel-forming reduction reactions with useful oxidative chemical transformations. Several studies have already demonstrated that electrons could be extracted from biomass, organic compounds and even plastics to produce H_2 with versatile light-absorbing systems.[65–69] Artificial photosynthesis systems reduce the dissipation of energy and electrons along the pathway, enabling high solar-to-fuel efficiencies routinely surpassing their natural counterparts.[70–73] Artificial photosynthesis is also empowered by an array of analytical techniques such as electrochemistry, spectroscopy and *operando* methodologies,[40,45,74,75] which are still less commonly employed for quantitative studies in biological research. The well-defined features of synthetic materials permit systematic investigations to understand reaction mechanisms and establish structure–function relationships for system design and optimisation.[76]

Semi-artificial photosynthesis provides a hybrid approach to solar-to-chemical conversion, by integrating the biocatalytic machinery (enzymes and microbes) with synthetic materials (dyes, electrocatalysts, semiconductors, electrodes, mediators).[77] The photosynthetic biohybrid systems seek to outsource tasks to the components that can perform them best and thus combine strengths of both while bypassing limitations of each. In such hybrid systems, enzymes and microbes function often as catalysts to drive endergonic and complex chemical reactions, whereas synthetic materials are commonly scaffolds to immobilise biocatalysts and functional components that carry out light absorption, charge transfer, chemical transformations and product separation. Several synthetic materials such as polymers and metal organic frameworks can also provide additional protection to fragile enzymes for more sustained operation against environmental stressors.[78–80] According to the form of biocatalyst,

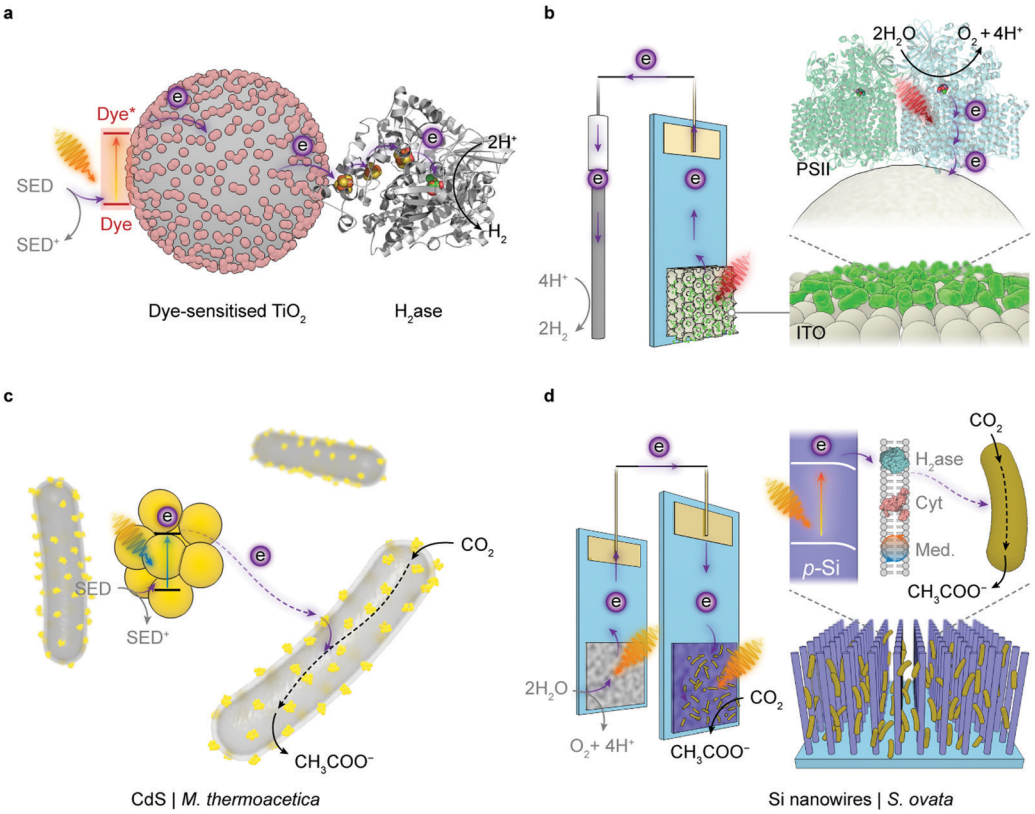

Fig. 5 Representative semi-artificial photosynthesis systems. (a) A colloidal system with dye-sensitised TiO_2 nanoparticles and H_2ase.[145] Under irradiation, the dye is excited and donates electrons to the conduction band of TiO_2. The photoelectrons are then delivered to the catalytic centre of H_2ase for proton reduction *via* intraprotein electron relays. The oxidised dye is regenerated by extracting electrons from a sacrificial electron donor (SED). (b) An electrode system with a three-dimensional indium tin oxide (ITO) electrode and PSII.[102,120] PSII is wired by the porous ITO scaffold and photocatalyses water oxidation, aided by an applied potential. (c) A colloidal system with light absorbing CdS nanoparticles deposited on the CO_2-reducing bacterium *M. thermoacetica*.[226] The excited CdS transfers photoelectrons to the bacterium, which generates reducing equivalents to produce acetate from CO_2 *via* the Wood–Ljungdahl pathway. The holes in CdS are quenched by the SED. (d) A hybrid tandem system with TiO_2 nanowires as the photoanode and p-Si nanowires integrated with acetogenic bacteria *S. ovata* as the photocathode.[248] When irradiated, the TiO_2 electrode oxidises water while p-Si nanowires generate photoelectrons that are delivered to the interfacing *S. ovata via* extracellular electron transfer pathways. *S. ovata* uses these electrons to reduce CO_2 into acetate through the Wood–Ljungdahl pathway.

semi-artificial photosynthesis falls into two categories: the enzymatic and the microbial system. Each of these systems can be further distinguished as either a colloidal suspension or a PEC cell (Fig. 5).

3 Enzymatic hybrid systems

An enzymatic hybrid system employs separated electroactive or photoactive enzymes as catalysts or light absorbers, to function in concert with synthetic components in driving reactions selectively at high rates and yields (Fig. 5a and b). Amongst a myriad of enzymes available in nature, only a handful of them are of interest in synthetic reactions starting from the simplest feedstocks (*e.g.*, H_2O, CO_2 and N_2). Translation of their catalytic ability *in vivo* into advantages *in vitro* is confronted with several challenges. Whereas synthetic catalysts are either integral parts of electrodes or discrete entities (particles or molecules), these redox enzymes are proteins with molecular weights of 10^4–10^6 g mol^{-1} and areal footprints of 50–400 nm^2. Their active sites (catalytic centres) are embedded within the protein matrices, which prevent indiscriminate reactions with substrate analogues. These enzymes have evolved intraprotein electron relays such as haems, quinones, and [Fe–S] clusters that can carry electrons between active sites and redox partners.[81] The electron relays define directional electron transfer pathways within the protein and allow electrochemistry to activate, monitor and modulate the enzymatic redox chemistry.[82] The current knowledge of the structure, functionality and catalytic mechanism within the enzymes discussed in this section has already been reviewed previously and is therefore not discussed here.[59,83–86]

To approach maximal catalytic rate, enzymes are expected to accelerate the chemical reactions towards diffusion controlled kinetics.[87] As such, enzymes should engage with electrodes in an "electroactive" orientation to enable rapid electron transfer kinetics between the distal relay centre and the electrode surface. In this regard, the enzyme–electrode interface must be rationally engineered with respect to topology, porosity and surface chemistry (hydrophilicity, surface charge, functional moieties, *etc.*). From a kinetic perspective, redox enzymes

reduce the activation energy and thus, minimise the electrochemical overpotential needed to drive a reaction.[59,88] Therefore, enzymes can often catalyse redox reactions very close to their thermodynamic potentials and reduce the energy penalty arising from large overpotentials. The low overpotentials can simplify system design by judiciously pairing with light absorbers and electron mediators according to their energy levels, and carry out reactions that were otherwise not possible with conventional electrocatalysts.

3.1 Water oxidation

Water is the "ideal" terminal electron source for the downstream fuel-forming reactions in artificial photosynthesis, but only few molecular catalysts with earth-abundant elements can handle this multielectron/proton process in an efficient fashion, which is further complicated by the combination with light absorbers. PSII, however, assigns the tasks of light harvesting and water oxidation to antenna proteins and the oxygen evolution centre (OEC), respectively, and orchestrates photochemistry in concert with catalysis in a stepwise manner *via* efficient intraprotein electron relays.[89] However, the intrinsic fragility of PSII under light irradiation limits the longevity of its catalytic activity ($\tau_{1/2}$ < 30 min) and thereby strangles the continuous downstream synthesis with isolated PSII.[90]

Antenna complexes in PSII harvest solar light and funnel the light energy to P680, where charge separation occurs within a few picoseconds.[91] This is followed by an electron transfer towards a pheophytin molecule (Phe_{D1}) and later to plastoquinone A (Q_A) (Fig. 6a). The resulting highly oxidising P_{D1}^+ in P680 can extract an electron from a redox-active tyrosine Y_Z (Tyr_Z) and then initiate water oxidation at the Mn_4CaO_5 cluster.[91] On the stroma side, Q_A is tightly bound to the D2 protein and acts as a single-electron acceptor, whereas Q_B in the D1 protein can accept two electrons and be fully protonated.[92] The charge transfer from Q_A to Q_B is aided by a non-haem iron midway between them.[93] The formed Q_BH_2 departs from the reaction centre and is replenished by the plastoquinone pool in the thylakoid membrane.

PSII is a biological model OER photocatalyst that inspires synthetic endeavours to mimic its core components,[61,94–96] and stimulates mechanistic investigations to understand its functionality.[97–99] Wiring PSII to an electrode allows the resulting biohybrid electrode to supply photoelectrons from water, and permits protein film-photoelectrochemistry (PF-PEC) to benchmark enzymatic activity *in vitro*, dissect photoinduced electron transfer pathways, and repurpose biogenic electrons to drive endergonic reactions.[90,100]

Attempts to interface PSII with an electrode surface started several decades ago,[101] when isolated PSII was deposited on a Pt electrode and generated a photocurrent of a few microamperes. However, the minuscule amount of PSII loaded on the electrode renders in-depth studies and proof-of-concept demonstrations unfeasible. Underlying PSII-PEC is the electrode that provides a physical scaffold to immobilise enzymes and an artificial electron acceptor for the biogenic electrons. PSII's photochemistry and the ensuing current output can be greatly influenced by the material, morphology and physical property of the electrode scaffold, which dictates the strength of protein binding, the capacity of protein loading, the accessibility to intraprotein electron relays, the depth of light penetration, and the transport of reactants and products therein.[102]

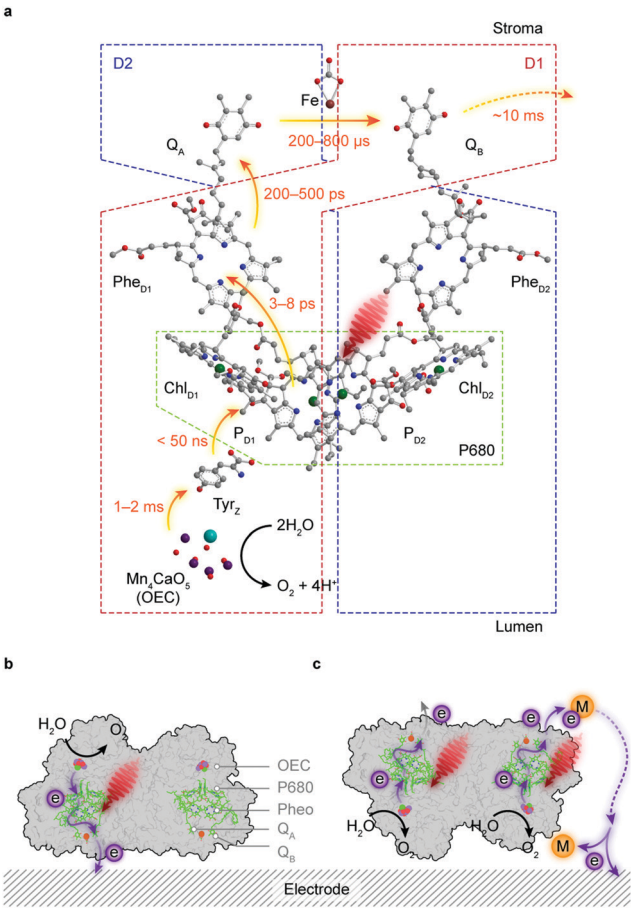

Fig. 6 Electron transfer pathways in PSII-photoelectrochemistry. (a) Schematic representation of the electron transfer pathways (indicated by the orange arrow) in the reaction centre complex of PSII. (b and c) Electron transfer at the PSII-electrode interface. Direct electron transfer can only take place provided that the stromal side of PSII intimately interfaces with the electrode (the electroactive orientation, b). PSII cannot donate electrons to the electrode in unsuitable orientations unless there are diffusional redox couples that can mediate electrons between Q_B and the electrode (c).

The directionality of the intraprotein electron flow makes the interfacial electron transfer highly dependent on the protein orientation. Q_B, the terminal electron acceptor in PSII, can only undertake outward electron transfer if the stromal side of PSII is in close proximity to an electrode surface (Fig. 6b). The electron transfer *via* intrinsic plastoquinones, namely, direct electron transfer (DET) can be registered as an anodic photocurrent by chronoamperometry under irradiation, and verified in control experiments by the removal of the Mn_4CaO_5 cluster or addition of 3-(3,4-dichlorophenyl)-1,1-dimethylurea (DCMU) that inhibits the Q_B site and interrupts the electron flow from Q_A.[103,104] DET often results in a relatively low photocurrent because PSII loading may be low and a significant portion of the enzymes may be in an unfavourable orientation or remote

from the electrode surface (Fig. 6c). This problem can be mitigated by using diffusional mediators such as 2,6-dichloro-1,4-benzoquinone (DCBQ, E_m = 0.32 V *vs.* SHE, pH 7.0) to shuttle electrons from the Q_B site to the electrode (Fig. 6c).[103] This mediated electron transfer (MET), in biological and artificial systems, comes at an expense in both energetics and kinetics, as extra energy is needed to drive the redox turnover of electron mediators and the diffusion of mediators is likely to govern the overall rate of electron transfer.

From both fundamental and practical viewpoints, an electrode with a large number of proteins being wired in an electroactive orientation is desired to produce a high photocurrent that can afford reliable analysis and proof-of-concept demonstrations (Fig. 7a). The making of such electrodes enables new possibilities to create solar-to-fuel pathways unattainable in biology. The chronology of the development of PSII electrode design will be outlined below.[100]

In the nascent stage of PSII-PEC, PSII with a polyhistidine tag (His-tag) at its stromal side was immobilised on flat Au electrodes by a self-assembled monolayer (Fig. 7b).[105–108] The interaction between electrode-anchored nickel-nitrilotriacetic acid and His-tags permitted site-selective binding of PSII on Au electrodes. However, the flatness of the electrode surface limited the protein loading typically below 10 pmol cm^{-2} and thus resulted in submicroampere photocurrents.[108] Electrodes using a redox polymer matrix as a non-diffusional mediator to electrically wire a high amount of proteins enable redox centres on the polymer backbone to access intraprotein electron relays, regardless of their orientations and distances (Fig. 7c).[109] A polymer with the Os^{3+}/Os^{2+} redox couple ($E_{1/2}$ = 0.39 V *vs.* SHE) was employed as both an immobilisation matrix and an electron mediator to PSII, which gave rise to a photocurrent density up to 45 μA cm^{-2}.[110]

The second generation of electrodes are mesoporous films made with metal oxides such as Fe_2O_3, TiO_2 and ITO.[104,111–115] A mesoporous ITO (meso-ITO) film with a thickness of 2–10 μm and a pore size up to 100 nm can be made with a high degree of tunability (Fig. 7d).[104,111,116,117] The meso-ITO afforded a PSII loading of 19 pmol cm^{-2}, which resulted in a DET photocurrent of 1.6 μA cm^{-2} and a mediated photocurrent of 22 μA cm^{-2}.[104] The surface chemistry of ITO can be modified to covalently bind PSII in favour of an electroactive orientation.[111] The meso-ITO film can also be deposited onto the disk of a rotating ring disk electrode to detect the O_2 production on the ring and study the oxygenic photoreactivity in PSII.[118]

The state-of-the-art third generation electrodes for PSII-PEC feature a hierarchical inverse opal structure with both macroporosity and mesoporosity (Fig. 7e).[102,119–127] This electrode architecture has interconnected macropores that provide a large surface area accessible by protein diffusion. The skeleton is made of a mesoporous structure consisting of (semi)conducting and hydrophilic nanoparticles (*e.g.*, ITO or TiO_2) where proteins are adsorbed. The inverse opal electrodes can be fabricated *via* a co-assembly method using polystyrene beads as the structural template and nanoparticles as the electrode material. Such method makes the electrode structure easily variable to fit biocatalysts with different dimensions.[128,129] The hierarchical structure also benefits both mass transport and light transmission, and permits high PSII loading in the range of 30–1000 pmol cm^{-2} (depending on the film thickness).[119–122]

A 40 μm thick inverse opal-ITO (IO-ITO) electrode with PSII attained a high photocurrent of 17 μA cm^{-2} for DET and 930 μA cm^{-2} in the presence of a DCBQ mediator.[120] Os-based polymers can further be incorporated in the IO-ITO scaffold to improve the electrical wiring between PSII and the electrode to eliminate the need for diffusional additives.[121] Compared to flat electrodes,[110] the IO-ITO electrode with the polymer matrix achieved a higher photocurrent of 381 μA cm^{-2} due to higher PSII (336 pmol cm^{-2}) loading.[121] The high photocurrent allowed for reliable O_2 quantification to calculate the Faraday efficiency, which was not possible with flat electrodes.

PSII immobilisation on porous ITO electrodes also allowed PF-PEC to dissect unexpected electron transfer pathways at the enzyme–electrode interface.[100] DET from Q_A to the ITO electrode

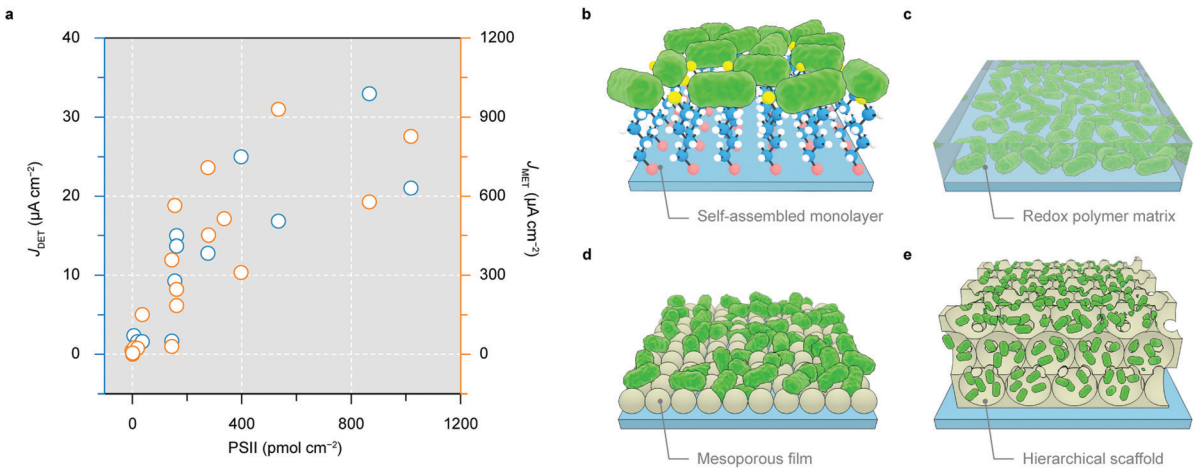

Fig. 7 Electrode architectures to wire PSII for semi-artificial photosynthesis. (a) Correlation between protein loading in electrodes and the resulting photocurrent by DET (blue dots, the left axis) and MET (orange dots, the right axis). (b–e) PSII wired to a flat electrode *via* a self-assembled monolayer (b), and a redox-polymer matrix (c); PSII immobilised in a mesoporous film with nanoparticles (d), and a three-dimensional hierarchical scaffold (e).

was observed when inhibiting PSII with DCBQ, showing the possibility to release electrons upstream of Q_B.[104,130] Furthermore, analysing cathodic current contributions at low potentials allowed identifying a competing pathway stemming from photo-induced O_2 reduction, presenting a short-circuit to the natural water oxidation process.[118,130]

Although PSII is the only enzyme that operates in nature for water oxidation to O_2, it is not the only enzyme that can perform this reaction *in vitro*. Laccase, a blue multicopper oxidase that couples the oxidation of organic substrates with the reduction of O_2 to H_2O, has been shown to catalyse the reverse water oxidation reaction when immobilised on an electrode ($E > 1.2$ V *vs.* SHE, pH 7.4).[131] In an attempt to use this enzyme for light-driven water oxidation, laccases were adsorbed on a semiconducting In_2S_3 electrode (band gap: 2.0 eV) as a visible-light absorber.[132]

3.2 Hydrogen production

H_2ases are metalloenzymes that can catalyse the interconversion between H_2 and H^+/e^- with a TOF of >1000 s^{-1}.[84,133] The HER activity of H_2ases per active site is therefore comparable with that of the benchmark Pt catalyst.[134,135] There are three phylogenic classes of H_2ases termed according to the metallic centres at their active sites: [NiFe]–H_2ase, [FeFe]–H_2ase and [Fe]–H_2ase, but only [NiFe]– and [FeFe]–H_2ases incorporate [Fe–S] clusters as electron relay centres and can catalyse the reversible proton reduction to H_2.[136] These [Fe–S] clusters are spaced 10–14 Å apart, which permits sequential electron tunnelling towards the active sites at a rate (10^7 s^{-1}) faster than catalysis.[137,138]

These intraprotein electron relays can couple the catalytic turnover at the active site with the electron exchange through the electrode, and thus enable protein film electrochemistry (PFE) to probe the H_2–H^+ interconversion by deciphering resulting voltammograms and chronoamperograms.[135,139] PFE reveals that [FeFe]–H_2ases are active for both proton reduction and H_2 oxidation yet extremely sensitive to O_2, whereas the more O_2-tolerant [NiFe]–H_2ases usually show strong catalytic bias towards H_2 oxidation and the reverse H^+ reduction is often susceptible to H_2 inhibition.[136]

[NiFeSe]–H_2ases are a subclass of [NiFe]–H_2ases with a selenocysteine residue coordinated to the nickel at the active site instead of a cysteine.[138] [NiFeSe]–H_2ases are kinetically more biased than other [NiFe]–H_2ases towards H_2 evolution without substantial product inhibition (Fig. 8i and j). The presence of selenium provides additional protection to the nickel centre from oxidative attacks, and hence confers better oxygen tolerance.[138,140,141]

[NiFeSe]–H_2ase is therefore a common model biocatalyst and has been rationally coupled with various light absorbers for photocatalytic HER (Fig. 8). Early attempts employed dyes to generate photoelectrons, which were carried to H_2ases by diffusional electron mediators such as methyl viologen (MV), in the presence of a sacrificial electron donor (SED).[142,143] A more recent study shows that an organic dye **Eosin Y** could directly transfer photoelectrons to [NiFeSe]–H_2ases without any electron mediators (Fig. 8a).[144] The homogeneous system produced 0.5 μmol h^{-1} H_2 for up to 15 h, corresponding to a TOF_{H_2ase} of 13.9 s^{-1}. Notably, this **Eosin Y**–H_2ase system also demonstrated some tolerance towards oxygen: more than 80% of photoactivity was retained with 5% O_2 and the system remained photoactive even at aerobic conditions (21% O_2) for 3 h. The system performance was limited by the interfacial electron transfer between dye molecules and H_2ases.

To this end, semiconductors were used as light absorbers with immobilised H_2ases. Photogenerated electrons can thereby stream directly from the conduction band towards the enzyme's distal relay centre (Fig. 8b). Co-adsorbing [NiFeSe]–H_2ases on **RuP**–TiO_2 particles through the putative interaction between the TiO_2 surface and side-chain carboxylates near the distal [Fe–S] cluster yielded 3.56 μmol H_2 in the first hour of irradiation and a benchmark TOF_{H_2ase} of 50 s^{-1}.[145,146] Replacing **RuP** with a metal-free diketopyrrolopyrrole (**DPP**) dye to sensitise TiO_2 also attained similar HER activity (Fig. 8b).[147] Likewise, [FeFe]–H_2ases were immobilised on CdTe nanoparticles or CdS nanorods that had their surfaces modified with 3-mercaptopropionic acid.[148,149] The negatively-charged surface induced [FeFe]–H_2ases to interface with the semiconductors at their positive patch close to the distal [Fe–S] cluster. Transient absorption spectroscopy elucidated that the electron transfer occurred between the conduction band of CdS and the distal [Fe–S] cluster in [FeFe]–H_2ase, regardless of the enzyme activity, at a rate ($\sim$100 ns) comparable with that of the charge recombination in CdS.[150] The rate of electron transfer is several orders of magnitude slower than that in synthetic systems (10^{-3}–1 ns),[151] probably due to the longer tunnelling distance (>10 Å) between the semiconductor surface and the distal [Fe–S] cluster. Nevertheless, the interfacial electron transfer is fast enough to outpace the incident photon flux, rendering the light absorption by CdS performance-limiting.[150]

The H_2 evolution rate of the above systems declined over a few hours, presumably due to dye degradation or an unstable material–enzyme interface. Thus, robust carbon-based light absorbers such as carbon nitride (CN_x) and carbon dots were utilised to improve the long-term stability (Fig. 8c).[152–154] The CN_x–H_2ase hybrids remained photoactive for 48 h, totalling 2.5 μmol of H_2 production and a turnover number (TON) of $>50\,000$.[152] But the weak interaction between CN_x and H_2ases rendered the TOF_{H_2ase} much lower (1.5 s^{-1}, in the first 4 h) than that of **RuP**–TiO_2–H_2ase hybrids. This problem can be partially resolved by blending CN_x with TiO_2 that has a high affinity for H_2ases.[153] The ternary hybrids exhibited better photocatalytic activity with a higher TOF_{H_2ase} of 7.8 s^{-1} within the first 4 h of irradiation and a longer H_2 evolution span of 72 h. The photostability of H_2ases was even better than their synthetic analogue, a molecular DuBois-type Ni bis(diphosphine) catalyst, that decomposed within 3 h of irradiation.[152] [NiFeSe]–H_2ases adsorbed on amine-capped carbon dots attained similar activity: a TOF_{H_2ase} of 1.1 s^{-1}, H_2 production of 2.6 μmol and a total TON of 52 000 in 48 h.[154] A comparison with carboxylic acid-capped carbon dots echoes with the previous finding that [NiFeSe]–H_2ases prefer to electrostatically interact with positive surfaces, and underlines the importance of semiconductor surface chemistry that controls the electronic communication with enzymes.[148,149,155]

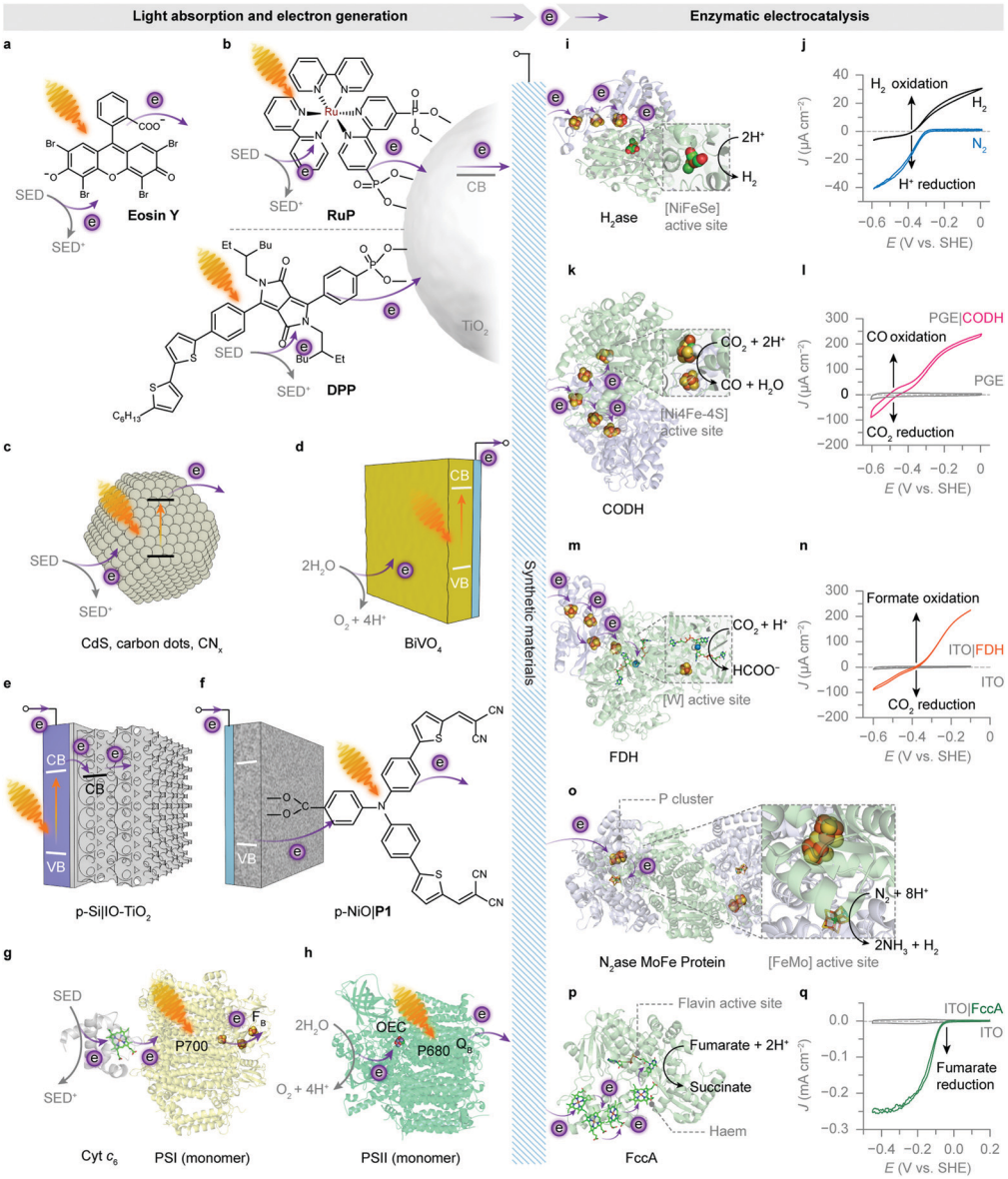

Fig. 8 Enzymatic hybrid systems for semi-artificial photosynthesis. (a–h) Light harvesting and low-potential electron generation by abiotic and biotic light absorbers. (i–q) Enzymatic electrocatalysis. (a) An excited xanthene dye **Eosin Y** (λ_{max} = 539 nm[297]). (b) Photoexcited electrons from the **RuP** or diketopyrrolopyrrole (**DPP**) dye are injected into the conduction band (CB) of TiO_2 and further directed to biocatalysts. (c) Irradiation of semiconducting particles, such as polymeric carbon nitride (CN_x), carbon dots and CdS, results in photoinduced electron transfer to biocatalysts. (d) A monoclinic $BiVO_4$ electrode absorbs light and generates photoelectrons while using water as the electron donor. (e) An IO-TiO_2 scaffold on a p-Si electrode as the photocathode for biocatalysts. Under irradiation, the excited p-Si electrode injects electrons into the CB of IO-TiO_2, which are further delivered to the interfacing biocatalysts. (f) A **P1** dye-sensitised p-type NiO electrode as the photocathode for biocatalysts. Light absorption by the **P1** dye provokes electron transfer from the valence band (VB) of NiO, followed by an electron injection into the biocatalysts adsorbed on the NiO scaffold. (g) The reaction centre chlorophylls (P700, λ_{max} = 700 nm) in PSI are excited by visible light irradiation. The photogenerated electrons are transferred to the terminal [Fe–S] cluster F_B *via* intraprotein electron relays. The luminal side of PSI is tethered with a cyt c_6. Shown here is the core complex of a PSI monomer (protein data bank ID: 5oy0). (h) An excited PSII monomer (protein data bank ID: 4ub6) transfers photoinduced electrons to the terminal electron acceptor (Q_B) at the stromal side. The generated holes oxidise water to O_2 at the OEC. (i) The protein structure of a [NiFeSe]–H_2ase (protein data bank ID: 1cc1). Exogenous electrons are delivered *via* [Fe–S] clusters to the [NiFeSe] active site for proton reduction. (j) Protein film voltammogram of H_2ase adsorbed on a TiO_2 electrode in N_2 or H_2, at pH 6.0. Reproduced from ref. 162 with permission from Wiley-VCH, copyright 2016.[162] (k) The protein structure of a CODH (protein data bank ID: 1jqk). Electrons are transferred *via* [Fe–S] clusters to the [NiFeS] active sites to drive the CO_2 reduction into CO. (l) Protein film voltammetry scans of CODH adsorbed on a pyrolytic graphite edge (PGE) electrode (control: a bare PGE electrode, grey trace) in CO_2/CO (50%/50%) at pH 6.0. Reproduced from ref. 159 with permission from the American Chemical Society, copyright 2013.[159] (m) The protein structure of a FDH (protein data bank ID: 1h0h). Electrons are transferred through the intraprotein [Fe–S] relays to the [W] active site for the reduction of CO_2 to formate. (n) Protein film voltammogram of reversible reduction of CO_2 to formate by an FDH-loaded mesoporous ITO electrode (control: a bare ITO electrode, grey trace) in CO_2/$NaHCO_3$ containing formate, at pH 6.5. Reproduced from ref. 193 with permission from Wiley-VCH, copyright 2019.[193] (o) The protein structure of a [MoFe] protein from N_2ase (protein data bank ID: 4wes). Exogenous electrons access the [MoFe] active site *via* a P cluster ([8Fe7S]) to transform N_2 into NH_3. (p) The protein structure of fumarate reductase (FccA, protein data bank ID: 1d4c). Haem cofactors function as intraprotein electron relays to direct electrons towards the flavin active site for fumarate reduction to succinate. (q) Protein film voltammogram of FccA adsorbed on an IO-ITO electrode (control: a bare IO-ITO electrode, grey trace) in 1 mM fumarate at pH 7.0. Reproduced from ref. 117 with permission from the Royal Society of Chemistry, copyright 2016.[117]

The aforementioned systems employ SEDs such as triethanolamine (TEOA) or ethylenediaminetetraacetic acid (EDTA) to expediently bypass the kinetic difficulty of water oxidation. To enable water to supply electrons for reductive reactions, synthetic chemistry and biology utilise different approaches. Artificial photosynthesis can carry out water oxidation separately by a photoanode in a PEC system. $BiVO_4$ has a band structure well-suited for solar water oxidation, but it is insufficient to reduce protons (Fig. 2 and 8d).[156,157] A photocathode hosting HER catalysts is thus required to further energise the electrons that are withdrawn from water by the $BiVO_4$ photoanode. The electrochemical window of ITO (−0.6 to +2 V *vs.* SHE, pH 7.0) limits its application at negative potentials needed to drive reducing reactions.[158] In view of this, ITO can be substituted with semiconductive TiO_2 to fabricate porous electrodes that are applicable under cathodic conditions.[159–161]

To this end, [NiFeSe]–H_2ases were interfaced with p-type silicon that was stabilised by a mesoporous TiO_2 layer.[162,163] The TiO_2 layer is necessary to protect the underlying p-Si from unwanted surface passivation,[163,164] but also to assist in binding [NiFeSe]–H_2ases. An ensuing problem is that enzymes having a large footprint show a low loading capacity on the mesoporous TiO_2 layer.[163,165] As such, a hierarchical IO-TiO_2 structure was built atop the p-Si to increase the H_2ase loading (up to 120 pmol cm^{-2}) (Fig. 8e).[166] A 4 nm TiO_2 interlayer was deposited on the surface of p-Si by atomic layer deposition to protect the electrode from the formation of an insulating SiO_2 layer, followed by the construction of the IO-TiO_2 scaffold. The p-Si|IO-TiO_2|H_2ase electrode gave a photocurrent onset potential of 0.0 V *vs.* SHE, pH 6.0, which is more positive than that of a water oxidising $BiVO_4$–TiCo photoanode (−0.1 V *vs.* SHE, pH 6.0). Thus the $BiVO_4$–TiCo||p-Si|IO-TiO_2|H_2ase tandem PEC system afforded overall solar water splitting without an external voltage, resulting in a stoichiometric production of H_2 (0.47 μmol, η_F = 98%) and O_2 (0.20 μmol, η_F = 84%) after 5 h of irradiation.[166] [FeFe]–H_2ases have also been interfaced with black Si electrodes with submicron porosity, but they are prone to desorb from the electrode surface due to weak interfacial interactions.[167]

Instead of using a p-type semiconductor, the H_2ase-loaded IO-TiO_2 scaffold was also interfaced with an encapsulated lead halide perovskite solar cell that generated a photovoltage of 0.9 V. In a tandem configuration with a $BiVO_4$–TiCo photoanode, the resulting system produced H_2 coupled to O_2 evolution with a STH efficiency of 1.1%.[168]

To streamline the electron transfer in biological H_2 production, photosystems and H_2ases could be directly wired *via* molecular wires, redox polymers, protein subunits or external circuits to eliminate the diffusion-governing steps.[18,120,166,169–171] For example, PSI has been connected with [FeFe]–H_2ases by 1,6-hexanedithiol to allow photogenerated electrons to tunnel between the two proteins (Fig. 8g).[18,169,172]

Alternatively, PSII and H_2ases were immobilised on IO-ITO electrodes and compartmentalised in a PEC cell (Fig. 8h).[120] The onset potential of an IO-ITO|H_2ase cathode (−0.4 V *vs.* SHE, pH 6.5) remained close to the thermodynamic value of proton reduction, whereas electrons from P680 were attenuated during the intraprotein electron transfer in PSII (Fig. 2). The energy is further offset by the use of electron mediators such as DCBQ that aid in the electron transfer from PSII to the electrodes. As such, a minimum bias voltage of 0.6 V was required to drive the photoelectrons from PSII towards H_2ase. At an applied voltage of 0.9 V, this biohybrid PEC cell (IO-ITO|PSII||IO-ITO|H_2ase) generated 0.52 μmol O_2 (η_F = 104%) and 0.96 μmol H_2 (η_F = 98%).[120] Note that the system performance with respect to photocurrent, onset potential and longevity was limited by the IO-ITO|PSII photoanode. To reduce the bias voltage in the future, one could possibly extract electrons from the upstream electron relays such as Q_A or pheophytin (Fig. 2).[104,130]

An easier way is to substitute for an electron mediator with a more negative redox potential than DCBQ whilst also introducing a second light absorber to reduce the bias voltage. This has been achieved by the use of 3,5-di-*tert*-butyl-1,2-benzoquinone (DTBoQ, E_m = 0.29 V *vs.* SHE) as the electron mediator, which shifted the photocurrent onset by 0.1 V earlier than DCBQ. When paired with a p-Si|IO-TiO_2|H_2ase photocathode, the required voltage was reduced to 0.24 V. At 0.4 V, the tandem PEC cell produced 0.125 μmol H_2 (η_F = 91%) within 3 h.[166]

At the anodic side, a second light absorber can be judiciously selected to imitate the function of PSI or to complement the light absorption of PSII. A working example is **DPP** that has a negative excited-state redox potential (−1.15 V *vs.* SHE) and strong light absorption between 400 and 550 nm (λ_{max} = 496 nm).[147] **DPP** and PSII were loaded in an IO-TiO_2 scaffold as the light absorbers and electrically connected by an Os-based redox polymer (P_{Os}) hydrogel.[119] Thus, a vectorial electron transfer from water to the TiO_2 electrode was established to prime electrons with sufficient reducing power for HER. Moreover, **DPP** conferred supplementary green-light absorption on this PSII-containing photoanode, thereby enabling a panchromatic sensitivity to visible light. By directly wiring the IO-TiO_2–**DPP**|P_{Os}-PSII photoanode with an IO-ITO|H_2ase cathode, autonomous solar water splitting can be carried out using wired enzymes without a bias voltage.[119] After 1 h of irradiation at zero bias, 0.015 μmol H_2 was detected with a Faraday efficiency of 76%. H_2ases at the cathode were not driven to their full capacity in catalysing proton reduction, due to the photodegradation of PSII *in vitro*. An initial applied bias STH conversion efficiency of 0.14% was obtained at a voltage of 0.3 V during the first hour.[119] PSI, the native second light absorber in the Z-scheme, has also been rewired with PSII and H_2ase by redox polymers in an attempt to reconstruct a biological H_2 production pathway *in vitro*.[173]

3.3 Carbon dioxide reduction

From a viewpoint of carbon products, the biomass produced by the Calvin cycle is not ideal to substitute for petrochemicals as feedstocks for the chemical industry.[174] However, biology has evolved more than one pathway for CO_2 fixation,[175] and the reductive acetyl-coenzyme A (acetyl-coA) pathway (Wood–Ljungdahl pathway) is an energy-conserving CO_2-fixing pathway, through which inorganic carbon is assimilated into cellular metabolism in the form of formate and CO by carbon monoxide dehydrogenase (CODH) and formate dehydrogenase (FDH).[176–178]

Both [NiFe]-CODH and metal-dependent FDH can catalyse the interconversion between CO_2 and their two-electron reduced carbon products, CO and formate, respectively. They control the binding of CO_2 and the transfer of electrons and protons to partition intermediates on the reduction pathway towards CO or its hydrated form, formate.[46]

[NiFe]-CODH is an O_2-sensitive metalloenzyme with a [NiFe]-active site from anaerobes such as *Moorella thermoacetica* and *Carboxydothermus hydrogenoformans* (Fig. 8k). It efficiently catalyses CO oxidation with a TOF up to 40 000 s^{-1} and CO_2 reduction with a TOF up to 45 s^{-1}, at a nearly thermodynamic potential (−0.5 V *vs.* SHE, pH 6.7) (Fig. 8l).[46,179,180] CO_2 is bound to the [NiFe]-cluster and undergoes a bifunctional attack by the electrophilic iron centre and the nucleophilic nickel centre, which enables a two-electron pathway for CO_2 activation.[181,182] Such two-electron reduction is also applied by [Mo]- or [W]-FDH, a metalloenzyme reversibly interconverting CO_2 and formate with minimal overpotentials (−0.39 V *vs.* SHE, pH 7.0) (Fig. 8m and n).[183,184] It has been determined that [W]-FDH isolated from *Syntrophobacter fumaroxidans* exhibited a TOF up to 3400 s^{-1} for formate oxidation and 280 s^{-1} for CO_2 reduction (with MV as the redox partner).[183] Both [W]- and [Mo]-FDH can achieve ~100% Faraday efficiency for electrocatalytic CO_2 reduction with formate as the sole product at modest overpotentials.[183,184] These enzymes provide an efficient two-electron CO_2 reduction pathway that bypasses the thermodynamically-uphill formation of $CO_2^{\bullet-}$.[185]

In view of the close thermodynamic redox potentials for CO_2/CO (−0.52 V *vs.* SHE, pH 7.0), proton reduction (−0.42 V *vs.* SHE, pH 7.0) and CO_2/$HCOO^-$ (−0.39 V *vs.* SHE, pH 7.0) (Fig. 2), similar strategies can be employed to drive CO_2 reduction with solar energy. [NiFe]-CODH was adsorbed on **RuP**–TiO_2 nanoparticles for light-driven CO_2 reduction to CO in the presence of an SED (Fig. 8b). During 4 h of irradiation, the **RuP**–TiO_2–CODH hybrids produced ~5 μmol CO, corresponding to an average TOF_{CODH} of 0.15 s^{-1}.[186] The relatively low turnover rate compared with H_2ase hybrids was partly due to a smaller driving force for CO_2 reduction than proton reduction, as the conduction band edge of TiO_2 (−0.52 V *vs.* SHE, pH 6.0) nears the thermodynamic potential for CO_2 reduction to CO. Factors such as interaction with TiO_2 and enzyme orientation also affect performance. The enzyme activity began to decrease after 3 h, and the low activity might be partly due to inefficient dye regeneration.[186,187] CODH has also been integrated in a PEC system comprising a **P1** dye-sensitised p-type NiO cathode (Fig. 8f).[188] The excited **P1** dye receives an electron from the valence band of the NiO electrode, followed by electron injection into an adjacent CODH, *via* intraprotein electron relay centres, down to its [NiFe]-active site, where CO_2 was reduced to CO (Fig. 8f).

Light-driven CO_2-to-formate conversion has been previously realised by FDH-based photoredox systems, where electrons from SEDs are energised by photosensitisers and delivered to FDH *via* electron mediators,[78,189–191] or by an FDH-based PEC system, where photoelectrons from the semiconductor photocathode p-InP were mediated to FDH by the MV/MV^{2+} redox couple.[192] The diffusional mediator can be eliminated by immobilising FDH on **RuP**–TiO_2 nanoparticles (Fig. 8b).[193] FDH showed a TOF of 11 s^{-1} in the first 6 h of photocatalysis and yielded 2.6 μmol formate.[193] Quartz crystal microbalance and infrared spectroscopy revealed that TiO_2 binds FDH strongly through both electrostatic interaction and chemisorption. FDH can also be wired with an electrode to work in tandem with a photoanode.[122,194,195] A recent study coupled an FDH-functionalised IO-TiO_2 cathode with an IO-TiO_2–**DPP**|P_{Os}-PSII tandem photoanode to drive CO_2-to-formate reaction with the aid of a small bias voltage.[122] After 1 h of irradiation with a bias of 0.3 V, 0.046 μmol of formate (η_F = 70%) was detected as the only product in the cathodic chamber of the PEC cell. The photocurrent decayed by half after 8 min, arising from the photodamage of PSII in the anode. Self-driven CO_2 reduction was recently achieved by a PV-PEC tandem system with a perovskite solar cell, a $BiVO_4$–FeOOH photoanode and a TiN nanoshell|FDH cathode.[194] The resulting PV-PEC tandem cell yielded formate at a rate of 1.06 μmol h^{-1} with a Faraday efficiency of 83% in 8 h, corresponding to a solar-to-fuel efficiency of 0.08%. The formate production could last for three days, and the decrease in activity was ascribed to the degradation of the perovskite solar cell outside the PEC cell. FDH can also be loaded on a TiO_2-deposited $CuFeO_2$–CuO photocathode to couple with a $BiVO_4$–FeOOH photoanode for autonomous light-driven CO_2 reduction.[196] This bias-free PEC cell allowed CO_2-to-formate conversion at a rate of 0.098 μmol h^{-1} with a Faraday efficiency of 33.5% in 8 h.

The product of CO_2 reduction can be extended from formate to methanol *via* an enzyme cascade.[197–199] A prototypical PEC system employed CoP_i-modified α-Fe_2O_3 and $BiFeO_3$ as the photoanode and photocathode, respectively, and contained a mixture of enzymes, *i.e.*, FDH, formaldehyde dehydrogenase and alcohol dehydrogenase, in the cathodic chamber.[198] Electrons extracted from water are energised by photoelectrodes and vectored through enzyme cascades to reduce CO_2 to methanol *via* NADH and diffusional electron mediators. Instead of being directly wired on the photocathode, enzymes in this system were dispersed in the catholyte, and depended on NADH, the reducing agent, to carry out redox reactions. As such, despite the well-aligned band positions, an external voltage (0.8 V) was needed to efficiently regenerate NADH and produce methanol (1.31 mM in 6 h).[198] An enzyme cascade was also immobilised in a silica matrix to work with an ''artificial thylakoid'' in a colloidal system.[199] The ''artificial thylakoid'' constituted a microporous protamine–TiO_2 hollow sphere (microcapsule) with CdS nanoparticles deposited on its luminal surface. The TiO_2 microcapsule received electrons from the excited CdS and exported electrons to regenerate NADH that furnished the enzyme cascade with reducing equivalents. In this way, photocatalytic oxidation and enzymatic CO_2 reduction were decoupled so that the enzymes were protected from photoinduced reactive oxygen species (ROS). This biohybrid system has demonstrated a high rate and yield in renewing NADH and thus generated 85 μM methanol from CO_2 in 2 h.[199]

3.4 Chemical synthesis

With enzymes as biocatalysts, photogenerated electrons from light absorbers can realise a broad spectrum of reactions of

synthetic interest, such as N_2 reduction, reduction of C=C bonds, formation of C–C bonds and hydroxylation of C–H bonds *etc.* Several recent studies are briefly highlighted here.

Biology converts N_2 into metabolically tractable NH_3 using N_2ases under physiological conditions. N_2ase is a two-component system comprising a [MoFe] protein and an electron-transfer [Fe] protein. The two proteins associate and dissociate during catalysis, sequentially delivering electrons and energy to the [MoFe] active site, where two NH_3 and one H_2 are generated from one N_2 and eight protons and electrons (Fig. 8o).[86] To leverage N_2ases for light-driven N_2 fixation, the isolated [MoFe] proteins were adsorbed on a CdS nanorod to form a biohybrid complex, where light energy replaces ATP hydrolysis to drive the enzymatic turnover in N_2.[200] The photoexcited CdS nanorods generated electrons with low reducing potential (−0.74 V *vs.* SHE, pH 7.0), which were then forwarded to the interfacing [MoFe] proteins for N_2 reduction. The CdS–[FeMo] protein hybrid attained an NH_3 production rate of 315 nmol $mg_{N_2ase}^{-1}$ min^{-1} and an average TOF_{N_2ase} of 1.25 s^{-1}. The NH_3 production lasted up to 5 h with a TON of 1.1×10^4 mol_{NH_3} $mol_{N_2ase}^{-1}$.[200]

The reduction of C=C bonds is exemplified by the conversion of fumarate to succinate, which can be catalysed by the flavoenzyme fumarate reductase (FccA) (Fig. 8p and q).[201] The light-driven fumarate reduction can be either performed in a colloidal system or within a PEC cell, using **RuP**-sensitised TiO_2 nanoparticles, and carbon dots or a W–$BiVO_4$–CoP_i electrode, respectively (Fig. 8b–d).[154,202] The FccA adsorbed on **RuP**–TiO_2 exhibited a TON of 5800 over 4 h of irradiation, corresponding to a TOF_{FccA} of 0.4 s^{-1},[202] while that on amine capped carbon dots achieved a similar TOF_{FccA} of 0.47 s^{-1} (averaged in the first 2 h of irradiation) with improved photostability up to 24 h.[154] Photoinduced enzyme degradation was likely to account for the slowdown of productivity. In a PEC system with a W–$BiVO_4$–CoP_i photoanode, the turnover rate of the immobilised FccA dropped down to ~0.01 s^{-1}.[202]

Another example is the use of old yellow enzymes (NADPH dehydrogenases) for stereoselective C=C reduction. Light absorbers including Au–TiO_2 or N-doped carbon dots were employed to produce photoelectrons that drive the regeneration of reducing equivalents such as NAD(P)H and its synthetic substitute, for *trans*-hydrogenation of conjugated C=C bonds.[203,204] With molecular xanthene dyes, photoelectrons could be directly transferred to the prosthetic flavin moiety in the old yellow enzyme, eliminating the need of using costly nicotinamide cofactors.[205] Such light-driven enzymatic catalysis yielded enantioselective products (enantiomeric excess > 90%) with conversion yields up to 80–90%.[204,205]

Photochemical C–C bond formation has recently been realised in a CdS–2-oxoglutarate:ferredoxin oxidoreductase (OGOR) hybrid system.[206] The OGOR catalyses the amalgamation of CO_2 and succinate into 2-oxoglutarate and is part of the reductive tricarboxylic acid cycle responsible for CO_2 fixation in many autotrophic microorganisms. The irradiated CdS generates reducing equivalents to drive the catalytic turnover at OGOR which involves large substrates, significant conformational changes during catalysis, and eventual formation of C–C bonds.[206]

Functionalisation of C–H bonds provides a straightforward and atom-economical access towards a plethora of organic products,[207] where enzymes such as cyt P450 show their synthetic advantages. The hallmark reaction of cyt P450 is the hydroxylation of C–H bonds, during which the delivery of electrons from the NADH reductase is synchronised with the activation of oxygen at the haem centre. The disadvantage of activity dependence on NADH cofactors and redox partners can be overcome by a semi-biological solution. A Ru(II)-diimine dye was covalently attached to a mutant haem domain of a cyt P450, which enabled excited dyes to inject electrons into the haem centre to catalyse the hydroxylation of lauric acid at an initial rate of 2.1 s^{-1} with a TON of more than 900 in 2 h, without the aid of NADH and reductase.[208]

4 Microbial hybrid systems

Microbial cells include an entire system of biochemical pathways and can produce metabolites of synthetic interest with high specificity at physiological conditions. Microorganisms utilise numerous enzyme cascades to maintain the intracellular metabolism. Different metabolic pathways are spatially organised to divert metabolites or enzymes that can react promiscuously, to maintain selectivity, concentrate reactants to drive unfavourable reactions, and protect enzymes or unstable intermediates from harmful cytoplasmic contents.[209] Moreover, these biosynthetic pathways are under dynamic regulation to keep cellular functionality in tune with physiological needs at different conditions. These features allow microbes to synthesise complex products from the simplest and stable feedstocks (*e.g.*, H_2O, CO_2, N_2, *etc.*) and render microbial catalysis resilient to environmental variations. Appealing to synthetic chemistry is their ability to produce multicarbon products from CO_2 *via* inherent carbon assimilation pathways such as the Wood–Ljungdahl pathway and the Calvin cycle.[175,178]

Such synthetic complexity is challenging to achieve with individual enzymes and a fixed reaction stoichiometry. Microbial catalysis can be further empowered by synthetic biology that employs genetic tools to access and engineer the intracellular metabolism, and create new pathways beyond the native metabolic pattern.[210] Compared with enzymatic counterparts, the microbial hybrid systems are less explored, but have provoked increasing interest in solar-to-chemical conversion, due to the possibility to synthesise complex chemicals, achieve better stability and prospects for scalability.[211,212] In the following discussions, we will summarise the recent achievements that take advantage of the microbial metabolism for chemical synthesis in solar energy conversion with photocatalysis and (photo)electrochemistry (Table 1).

Whereas enzymes catalyse biochemical reactions with specific substrates, products and stoichiometry, microorganisms are more versatile due to a set of diverse metabolic pathways involving a multitude of enzymes. Moreover, the microbial hybrid systems are being developed to establish an efficient conversion strategy of solar energy to desired multicarbon chemicals, a catalytic prospect particularly suitable for microorganisms.[213]

Table 1 Summary of selected microbial hybrid systems for solar-to-chemical conversion

Microbe	Light absorber	Microbial reaction	Ref.
E. coli	TiO_2	$H^+ \rightarrow H_2$	221
E. coli	CdS	$H^+ \rightarrow H_2$	222
R. capsulata	Bi_2O_3	$H^+ \rightarrow H_2$	218
R. capsulata	dye-TiO_2	$H^+ \rightarrow H_2$	219
R. eutropha	PV	$CO_2 \rightarrow$ biomass, isopropanol	240
M. barkeri	CdS	$CO_2 \rightarrow$ methane	225
M. barkeri	TiO_2/InP	$CO_2 \rightarrow$ methane	239
M. thermoacetica	CdS	$CO_2 \rightarrow$ acetate	226
M. thermoacetica	Au	$CO_2 \rightarrow$ acetate	231
M. thermoacetica	PDI/PFP	$CO_2 \rightarrow$ acetate	234
S. ovata	Si nanowires	$CO_2 \rightarrow$ acetate	248
S. ovata	Si nanowires	$CO_2 \rightarrow$ acetate	250
Clostridium sp.	PV	$CO_2 \rightarrow$ butanol, hexanol	212
R. palustris	CdS	$CO_2 \rightarrow$ PHB, carotenoids	232
S. cerevisiae	InP	Glucose $\rightarrow$ shikimic acid	238
G. sulfurreducens	$BiVO_4$	Fumarate $\rightarrow$ succinate	262
X. autotrophicus	PV	$N_2 \rightarrow NH_3$	243

Thus, we summarise progress for microbial hybrid systems from a different perspective: instead of organising this section by individual reactions enabled by such systems, we put the emphasis on key questions imperative for research in this field: how microorganism and synthetic materials are integrated into hybrid structures, how non-photosynthetic microbes are empowered with light-absorbing capabilities, and how fluxes of reducing equivalents are guided into intracellular metabolic pathways.

4.1 Microbial photocatalysis in colloidal systems

The discussion begins with the microbial hybrids operating in colloidal systems (Fig. 5c). We consider the HER as a model reaction in the context of solar-to-fuel conversion. Photosynthetic H_2 production can transiently take place in nature by microalgae and cyanobacteria under anaerobiosis, during which electron flux on the photosynthetic chain is shifted away from its normal path towards H_2ase.[17,214] However, such process is O_2-sensitive and competes with NADPH-dependent biological processes. Although the O_2-sensitivity can be partially alleviated by protective encapsulation,[215,216] the rate and yield of H_2 evolution are intrinsically limited by the light reaction, which saturates at fairly low light intensities (10–20% of solar light).[214] Whereas these drawbacks can be partially overcome by streamlining the solar-to-H_2 pathway with isolated H_2ases and light absorbers, laborious purification and fragility of the enzymes diminish the practicality of this approach.

An alternative are microbial hybrids where non-photosynthetic live cells are employed as biocatalysts, and the task of light harvesting is outsourced to synthetic light absorbers. Several early studies illustrate this strategy: H_2ase- (and N_2ase-) containing bacteria such as *Clostridium butyricum*, *Rhodopseudomonas capsulata*, *Rhodospirillum rubrum* were coupled with semiconductor nanoparticles, specifically, TiO_2 and Bi_2O_3 *via* MV as the electron mediator (Fig. 9a). In the presence of SEDs, photogenerated electrons were delivered into cells where H_2 evolved.[217–219] The low growth rate of these bacteria limits the availability of biocatalysts. As such, *Escherichia coli* (*E. coli*), a well-established bacterial chassis for synthetic biology,[220] was engineered to heterologously express genes encoding [FeFe]–H_2ases from *Clostridium acetobutylicum*.[221] The recombinant *E. coli* was mixed with TiO_2 nanoparticles and MV, and such hybrid system produced 216 μmol H_2 during 15 h of irradiation.

To enable visible light absorption, CdS was employed, and instead of inducing heterologous expression of [FeFe]–H_2ases, *E. coli* can produce H_2 in anaerobic conditions with endogenously synthesised [NiFe]–H_2ases. Moreover, CdS nanoparticles were precipitated on the bacterial surface to directly supply photoelectrons without diffusional mediators (Fig. 9b).[222] It has been found that photogenerated electrons interacted with the intracellular metabolism and guided more reducing equivalents along the pathway for H_2 production. To extend its aerobic uses, the CdS–*E. coli* hybrid was further encapsulated with biomimetic silica to protect the bacterium from oxygen.[216] Under aerobic conditions, the hybrid system continuously produced H_2 within 96 h of irradiation.

The catalytic ability of microorganisms is better exemplified in CO_2 reduction, where they can produce complex organic products not readily accessible through synthetic methods.[211] One example is CO_2 reduction to CH_4, which involves eight electron transfers that can facilely diverge to form a wide range of products.[223] In the realm of biology, this reaction is handled by methanogenic archaea as part of their energy-conserving metabolism.[224] In light of this, *Methanosarcina barkeri* (*M. barkeri*), an anaerobic methanogen, was employed as the catalytic machinery for CO_2-to-CH_4 conversion.[225] Like the aforementioned CdS–*E. coli* hybrids,[216,222] CdS nanoparticles were deposited on the surface of the *M. barkeri* as the light absorber. Photoelectrons produced by the excited CdS were delivered to the intracellular pathways *via* membrane-bound cytochromes or H_2ases and were used by the bacteria for methanogenesis (Fig. 9b). The CdS–*M. barkeri* hybrid produced 13.7 μmol CH_4 after three-day irradiation with a quantum efficiency of 0.34%.[225] Isotopic labelling experiments confirmed that the CH_4 was derived from CO_2 reduction. The CH_4 evolution halted after three days, likely due to the depletion of the SED cysteine.

CdS nanoparticles can also be interfaced with *Moorella thermoacetica* (*M. thermoacetica*), an acetogenic and electrotrophic bacterium. *M. thermoacetica* could directly use photogenerated electrons from the excited CdS to reduce CO_2 into acetate *via* the intracellular Wood–Ljungdahl pathway, while holes produced by CdS were quenched by cysteine (Fig. 9b).[226] A peak quantum yield of 2.44% was recorded at low-intensity simulated sunlight, which is comparable to the year-long averages ($\sim$0.2–1.6%) for plants and algae.[227]

The electron transfer pathways between CdS and *M. thermoacetica* was further elucidated by transient absorption spectroscopy: photoelectrons were transported *via* membrane-bound electron acceptors such as cytochromes, ferredoxin, flavoproteins and menaquinones at the initial stage (3 h) of photosynthesis; at longer duration (24 h), a membrane-bound H_2ase-mediated pathway dominated, which correlated with increased rates of acetate generation and thus a higher quantum efficiency.[228] A latest proteomic study revealed that the photoexcited CdS induced changes to the metabolic pattern of *M. thermoacetica*: a host of enzymes associated with the tricarboxylic acid cycle and glycolysis were up-regulated. Both pathways together with the

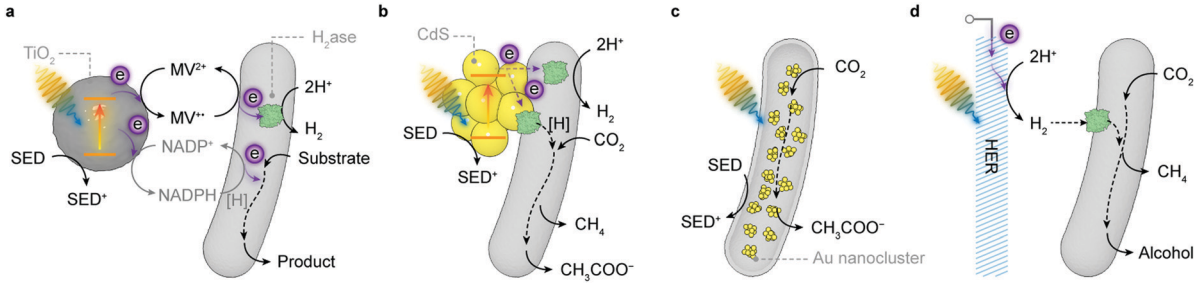

Fig. 9 Photosynthetic microbial hybrid systems. (a) Irradiated semiconducting nanoparticles (*e.g.*, TiO_2) transfer photoexcited electrons to microbes to produce H_2 or other products *via* the MV^{2+}/MV^{+} or $NADP^{+}$/NADPH redox couples in the presence of a SED. (b) CdS nanoparticles are deposited on the surface of microbes and deliver photoelectrons directly to the intracellular pathways for solar-to-chemical conversion and oxidise the SED under illumination. (c) Au nanoclusters are absorbed by microbes as intracellular light absorbers. Photoinduced electrons are delivered by cytoplasmic redox mediators to the Wood–Ljungdahl pathway that reduces CO_2 into acetate. (d) Microbes are introduced in the cathodic chamber of an electrolyser and leverage the produced H_2 as the reducing equivalents to transform CO_2 into CH_4 or multicarbon alcohols.

Wood–Ljungdahl pathway constitute the energy-conservation scheme of the CdS–*M. thermoacetica* hybrid system.[229]

To make the hybrid system more sustainable, the added cysteine, the SED to CdS, could be regenerated photocatalytically by TiO_2 nanoparticles loaded with Mn(II) phthalocyanine co-catalysts, which ultimately extracted electrons from water and delivered them to the CdS–*M. thermoacetica* hybrids *via* the cysteine/cystine redox couple.[230] The light absorbers can be replaced with those that are more biocompatible and accessible, for example, Au nanoclusters.[231] Au nanoclusters could be ingested by *M. thermoacetica* and directly deliver photoexcited electrons with longer lifetime to the Wood–Ljungdahl pathway *via* cytoplasmic redox mediators (Fig. 9c). The intracellular interplay between photochemistry and metabolism bypassed kinetic and energetic drawbacks stemming from transmembrane diffusion. The Au nanoclusters also could reduce ROS formed during irradiation, thus improving the cellular viability in this hybrid system and increasing acetate production with a higher quantum yield of $\sim$2.9%.[231]

A similar protocol is applicable to various microorganisms with different physiological functionality. For example, CdS nanoparticles were precipitated on the photosynthetic bacterium *Rhodopseudomonas palustris* for CO_2 fixation.[232] Under visible light, the excited CdS generated additional reducing equivalents for the innate Calvin cycle, which promoted the production of biomass and valuable multicarbon compounds such as carotenoids and poly-β-hydroxybutyrate (PHB), as well as the photosynthetic efficiency. When CdS was hybridised with *Thiobacillus denitrificans* (*T. denitrificans*), an autotrophic denitrifier, the resulting CdS–*T. denitrificans* hybrid could use the photoelectrons for NO_3^- reduction to N_2O.[233]

In light of its cytotoxicity, CdS has been substituted with organic semiconductors, *i.e.*, perylene diimide derivative (PDI) and poly(fluorene-*co*-phenylene) (PFP) as the photosensitiser.[234] PDI and PFP could be immobilised on the surface of *M. thermoacetica* through electrostatic and hydrophobic interactions, which enabled efficient electron transport across the cellular membrane. Such microbial hybrid system registered a quantum efficiency of 1.6%.

Light-driven fumarate reduction to succinate has been achieved by an enzymatic hybrid system with flavoenzymes (FccA),[154,202] but such reaction can also be accomplished by a dye-sensitised whole cell containing flavocytochromes.[235] This hybrid system comprised of photosensitisers (**Eosin Y** or proflavine), *Shewanella oneidensis* MR-1 (*S. oneidensis*), an electron mediator (MV) and a SED. Another model reaction is C–H bond functionalisation. Cyt P450 was employed to catalyse the hydroxylation of lauric acid with a covalently attached Ru(II) light absorber that was meant to deliver photoelectrons to the haem domain without the need of redox partners.[208] The same strategy also applies in a microbial hybrid system: the cyt P450 was expressed in an engineered *E. coli* bacterial chassis and **Eosin Y** was absorbed into the cytoplasm and directly bound to the haem domain of the enzyme.[236] Under visible light irradiation and with an SED, photoexcited **Eosin Y** can continuously supplement electrons to sustain the catalytic turnover of the cyt P450 more than 18 h (average TOF_{P450}: 2.5×10^{-4} s^{-1}).[236]

A comparison with the previous P450–Ru(II) dye hybrids illustrates the disparity that epitomises general differences between enzymatic and microbial systems. First, the P450–Ru(II) dye hybrids need post-translational modification to link the Ru(II) dye molecule to the specific cysteine residue, and such modification is specific to a particular type of cyt P450 and may affect the activity when applied to different cyt P450 variants.[208] In contrast, the whole cell system has demonstrated success with both bacterial and human cyt P450 in producing high value chemicals such as drugs and steroids.[236] Lastly, the enzyme hybrids showed an initial TOF_{P450} (2.1 s^{-1}) several orders of magnitude higher than the whole cell system, but the activity of the former began to languish within 2 h (average TOF_{P450}: 1.25×10^{-3} s^{-1}), while productivity of the latter can be compensated by the prolonged longevity ($>$18 h) and the increased quantity of biocatalysts.[208,236]

Besides bacteria, eukaryotic cells such as yeasts are also favoured as a platform cell factory for biosynthesis of fuels and chemicals, as their well-studied biology primes genetic and analytical tools to unravel the mechanisms governing electron transport and metabolic flux in biohybrid systems.[64] The intracellular redox reactions are dependent on cofactors, namely NADH or NADPH, as hydride sources and their generation is strongly intertwined with the central carbon metabolism.[237]

The expense of NAD(P)H precludes a stoichiometric supply to sustain the biosynthesis, and an effective cofactor regeneration was achieved photocatalytically by hybridising the yeast strain *Saccharomyces cerevisiae* (*S. cerevisiae*) with semiconducting InP nanoparticles (Fig. 9a).[238] *S. cerevisiae* was genetically engineered to suppress the cytosolic synthesis of NADPH and to enhance the carbon flux towards shikimic acid production. The NADPH was regenerated by the inward electron transport by irradiated InP nanoparticles bound on the cell surface. A maximum light-to-chemical conversion efficiency of 1.58% was attained within 12 h of irradiation.[238]

4.2 Electrolysis coupled to homogeneous microbial synthesis

Another biohybrid system integrated planktonic *M. barkeri* with a PEC cell system consisting of a water oxidising TiO_2 photoanode and a p-InP–Pt photocathode, to couple artificial H_2 evolution with biological methanogenesis. The unassisted water splitting under irradiation generated H_2 in the cathodic chamber, which was consumed by the methanogens therein as reducing equivalents to reduce CO_2 to CH_4 (Fig. 9d). This hybrid system produced 68.8 nmol CH_4 over three days, corresponding to a Faraday efficiency of 74%.[239]

Similar strategies can be extended to other strains of bacteria to obtain CO_2-reducing products that are more feasible for storage and transport.[240,241] For example, in a water electrolyser inoculated with genetically-engineered *Ralstonia eutropha*, a water oxidising CoP_i anode and a Co–P alloy cathode worked together at an applied voltage of 2.0 V to furnish the bacteria with H_2.[241] The bacteria transformed CO_2 and H_2 following a desired route into an array of fuels and chemical products such as poly(3-hydroxybutyrate), isopropanol, isobutanol and 3-methyl-1-butanol (Fig. 9d). The energy input can be readily outsourced to a photovoltaic device with a routinely attained efficiency of 18%,[2] and the resulting system could anticipate a solar-to-chemical conversion efficiency of $>7\%$.[241,242] Such a modular platform has furthermore been leveraged beyond CO_2 reduction, towards more complex ambient NH_3 synthesis from N_2 and H_2O with the H_2-uptake diazotrophic microorganism *Xanthobacter autotrophicus*.[243] In the above hybrid systems, H_2 acted as the vector of reducing power to connect microbial metabolism with artificial electrolysis. However, the low solubility of H_2 (0.79 mM, 25 °C) and inefficient H_2 delivery from the electrode limit the rate of throughput. A recent study shows that this bottleneck can be alleviated by introducing perfluorocarbon nanoemulsions as biocompatible H_2 carriers to increase the H_2 availability around cells, accelerate the H_2 transfer and thereby improve the productivity of CO_2 reduction.[244]

4.3 Photoelectrosynthesis with immobilised microorganisms

Instead of suspending microbes in solution, they can also be immobilised on electrodes to catalyse redox reactions driven by light or electricity (Fig. 10a). Such systems are referred to as microbial (photo)electrosynthesis. Underlying this process is the electron exchange ability of microorganisms with the interfacing electrode (Fig. 10b–d).[245] This can either occur directly between the electrode and microorganism or be mediated by H_2 and diffusional redox couples. The direct electron transfer for microbial electrosynthesis has the advantage of bypassing the handicap of low solubility of H_2 and the diffusional limitations of electron shuttles. Besides, it avoids the potential loss from intermittent H_2 generation and the potential toxicity of some mediators (*e.g.*, MV).[246]

From a practical perspective, the advantages over a planktonic system largely resemble the benefits of heterogeneous catalysis over homogeneous systems such as easy catalyst separation and recycling. One can readily and flexibly apply the microbial electrode for photosynthesis, either by pairing with a photoelectrode in a PEC cell or connecting with a solar cell for PV-driven electrolysis. Of more interest to fundamental studies is that the hybrid electrode system permits electrochemical toolsets to access the intracellular redox chemistry *via* the current exchange at the biointerface.

Oxygenic photosynthetic microorganisms such as cyanobacteria have been immobilised on IO-ITO electrodes with tailored porosity to perform semi-artificial photosynthesis.[128,129] The cyanobacterium encloses the entire photosynthetic apparatus within the cell, rendering themselves more robust than isolated PSII to carry out light-driven water oxidation. The cyanobacterial biofilm produced much lower photocurrent densities than those of PSII, but with increased longevity (>5 days).[128] Compared with the IO-ITO|PSII electrodes, the IO-ITO|biofilm systems exhibited different photocurrent profiles, which is derived from different electron transfer mechanisms at the interface. The cyanobacterium likely relies on intracellular redox mediators that are released under irradiation to carry electrons towards the electrode surfaces.[247]

There are only few reports to directly interface non-photosynthetic microorganisms with photoelectrodes.[248,249] The difficulty is in part due to the large footprint of cells, which requires appropriate electrode geometry to achieve a high loading density while maintaining light penetration. A notable example is an array of Si nanowires that served both as a light-absorbing semiconductor and a physical scaffold for the acetogenic bacterium, *Sporomusa ovata* (*S. ovata*) (Fig. 5d).[248] The bacteria were integrated with the Si nanowires by taking photoexcited electrons from the conduction band to sustain their metabolism. The resulting biohybrid electrode was assembled with a photoanode made of water oxidising TiO_2 nanowires for autonomous photoreduction of CO_2 to acetate. The PEC cell produced a stable photocurrent of 0.3 mA cm^{-2} for more than 120 h, yielding an acetate titre of 20 mM with a Faraday efficiency of 86%. The overall solar-to-chemical conversion efficiency registered 0.38% during 200 h operation. Acetate could further be activated into acetyl-coA, a common biochemical intermediate, to access a variety of biosynthetic fine chemicals. The downstream synthesis could be performed by genetically-engineered *E. coli* that transformed acetate into *n*-butanol, polyhydroxybutyrate polymer, and isoprenoid compounds.[248] Recently, the acetate production was accelerated as a result of a larger bacterial population and a better bacterium-nanowire interface, which was realised by improving the local pH environment inside the electrode.[250] As such, the solar-to-chemical conversion efficiency was increased to 3.6% over seven days when coupling to a photovoltaic device.

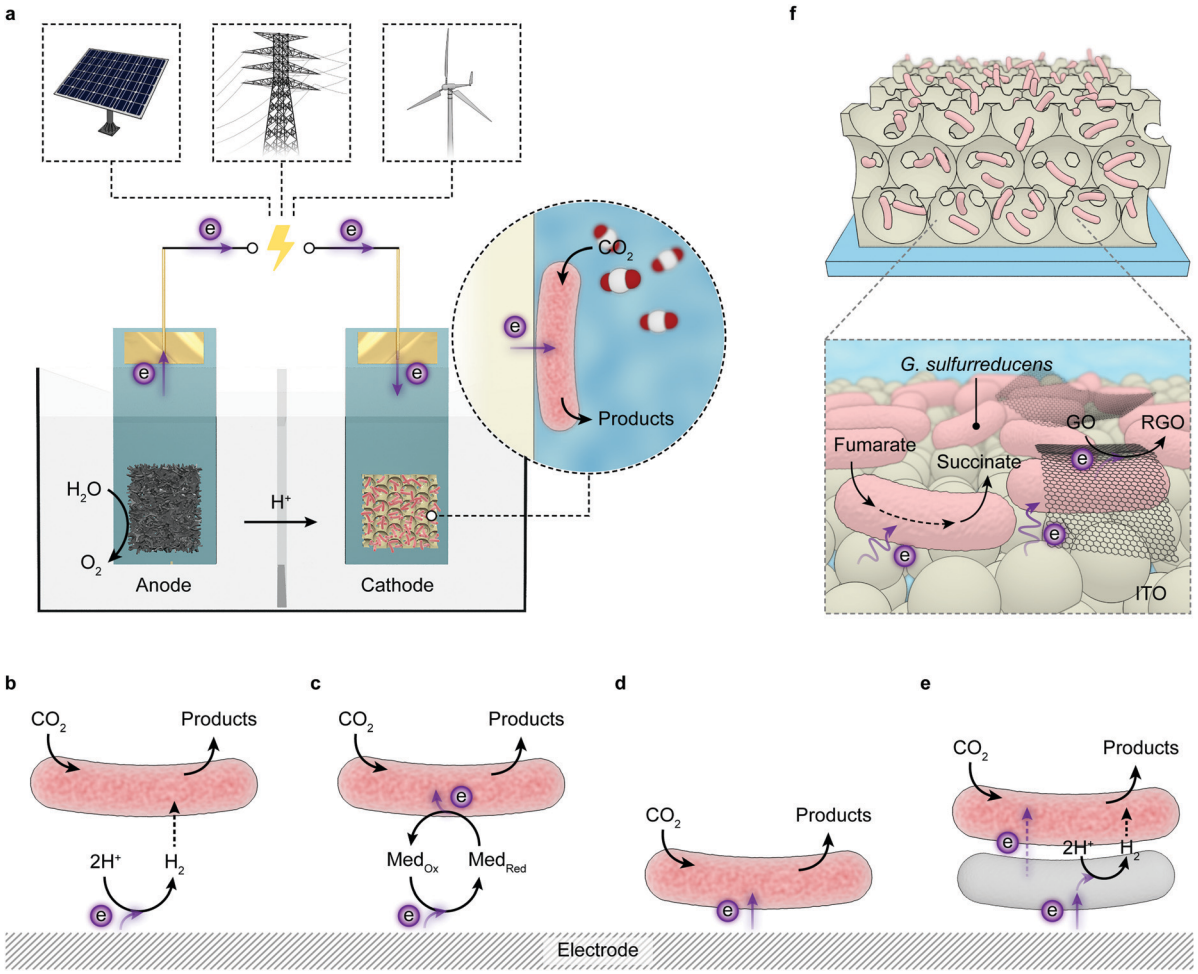

Fig. 10 Microbial electrosynthesis. (a) Schematic representation of a microbial electrosynthetic cell powered with electricity that can be derived from renewable sources (solar light, wind, *etc.*). At the anode chamber, an electrode donor (*e.g.*, H_2O) is oxidised, providing electrons. The cathode chamber contains a microbial hybrid electrode where microorganisms receive electrons from the interfacing electrode scaffold and drive the reduction reaction (*e.g.* CO_2 reduction). (b–e) Mechanisms for electron transfer from electrodes to microorganisms. Electrons from the electrode can be delivered to the microorganisms by H_2 (b), redox mediators (Med), (c), direct electron transfer (d) or *via* interspecies electron/H_2 transfer (e). (f) An IO-ITO|*G. sulfurreducens* hybrid electrode, in which *G. sulfurreducens* can directly receive electrons from the cathode and reduce fumarate or graphene oxide (GO). Reproduced from ref. 262 with permission from the National Academy of Sciences of the United States of America (NAS), copyright 2020.

Few light-absorbing semiconductors have been optimised to fit the dimension of microorganisms. Integration of microbes into the electrode scaffold also poses challenges on the chemical stability, biocompatibility, conductivity and surface chemistry of the semiconducting materials, not least the impact on light transmission. A simpler strategy is to immobilise microorganisms on electrodes with tailored morphologies while outsourcing light harvesting to photoanodes or external PV devices. This approach decouples light absorption from microbial metabolism, and thereby suppresses unwanted parasitic reactions and eliminates possible oxidative stresses stemming from photoinduced ROS. The simplified design also grants more flexibility in the making of electrode architectures to enhance the loading capacity and engineer the electrode surface to improve the interaction. Therefore, more efforts converge on interfacing microbial cells with tailored electrodes and improving the interfacial electron transfer and mass transport. Such exploitation can capitalise on decades of research in microbial fuel cells,[251] and be guided by recent understandings of the interaction between synthetic materials and microorganisms.[252,253] As these hybrid electrodes can readily operate with light absorbing electrodes or devices, to broaden the scope of discussion, this section will continue with a survey of recent progress in microbial electrosynthesis, where sessile bacteria exchange electrons with electrodes and carry out synthetic reactions.

An early study of microbial electrosynthesis employed graphite electrodes to supply *Geobacter sulfurreducens* (*G. sulfurreducens*) with electrons for fumarate reduction.[254] This is reminiscent of a previously described electrode–bacterium hybrid system, where H_2 acted as the electron vector (Fig. 10b). Yet this scenario has been ruled out because the electrode barely produced H_2 at the applied potential (−0.3 V *vs.* SHE, pH 6.8). Instead, *G. sulfurreducens* was able to directly receive electrons from the electrode (Fig. 10d).[255] The same reaction could also be accomplished by *S. oneidensis*

cultured on a graphite electrode or in a three-dimensional reduced graphene oxide (RGO) scaffold.[256,257]

An envisioned application for microbial electrosynthesis is bioremediation, namely, decontaminating the wastewater possibly powered by solar energy.[258] For example, under applied negative potentials, *G. sulfurreducens* could precipitate soluble U(VI) ions on electrodes, which can be easily collected.[259] Bacteria such as *Geobacter lovleyi* and *Anaeromyxobacter dehalogenans* with the ability to respire with chlorinated compounds can also be exploited to dechlorinate contaminants (*e.g.*, tetrachloroethene, 2-chlorophenol) in this manner.[260,261]

More recently, an IO-ITO electrode scaffold was employed to culture a large population of *G. sulfurreducens* (Fig. 10f).[262] The resulting biohybrid electrode catalyses the reduction of soluble fumarate and heterogenous graphene oxide (GO), with electrons from an external power source or an irradiated dye-sensitised (**RuP**–TiO_2) or water oxidising $BiVO_4$ photoanode.[262] The microbe-modified IO-ITO electrode enabled high current densities and also served as a platform underpinning a variety of analytical methods to decipher the electrical interplay at the biointerface.[263]

However, *Geobacter* and *Shewanella* strains lack CO_2-fixation pathways. Autotrophic microorganisms that can source energy from inorganic chemical reactions (chemolithotrophs) or light (photoautotrophs) for carbon assimilation are more promising in this regard, as they can adapt to use an electrode as the electron donor to generate reducing power.[264] Acetogens such as *S. ovata*, *Clostridium ljungdahlii*, and *M. thermoacetica* have been shown able to directly receive electrons from electrodes and reduce CO_2 into acetate with Faraday efficiencies of $>80\%$. Moreover, the electron uptake and CO_2 fixation can also be decoupled using two bacteria strains (*Acetobacterium woodii* and *Desulfobacterium corrodens*), which can separately receive electrons from the electrode and reduce CO_2, respectively, and communicate by means of interspecies H_2 transfer (Fig. 10e).[265]

As microbial electrosynthesis systems are anticipated to operate together with PV devices, the ultimate solar-to-chemical efficiency will to a large extent depend on the biochemical pathway that dictates the energetics and stoichiometry of the substrate–product conversion. Whereas a sulphur-oxidising phototroph *Prosthecochloris aestaurii* can sustain its photosynthesis with electrons supplied from a cathode,[266] its application for photoelectrosynthesis is largely unfeasible because the Calvin cycle is rather inefficient for solar fuel production and genetic tools to expand their synthetic diversity are not yet developed for some less studied microorganisms. Compared with methanogens of which CH_4 is the only attainable product, acetogens enable a wide repertoire of chemicals such as ethanol, isopropanol, *n*-butanol and 2,3-butanediol, which can be further extended by metabolic engineering.[267,268]

The alliance of microbial metabolism with photocatalysis and (photo)electrochemistry is formed by virtue of the translocation of reducing power from abiotic materials to biotic entities. This can be achieved by interfacing microorganisms with light absorbers/electrodes, where electrons are either directly transferred to microorganisms or shuttled inward *via in situ* generated electron carriers (*e.g.* H_2). Alternatively, electrons can be delivered to planktonic cells by diffusive redox mediators. Sessile microorganisms on electrodes can manage a high Faraday efficiency up to 90%. Yet the slow electron uptake (typically < 1 mA cm^{-2}), stemming from the kinetic disparity between the electrochemical and biochemical processes, which is less amenable to improvement by interface engineering, diminishes the economic feasibility of this approach.[269] Thus a technically favoured strategy may be to decouple the extracellular electrochemistry and intracellular biochemistry in a modular fashion, as exemplified by a recent microbial electrosynthesis setup that combined PV, electrolysis and fermentation modules.[212] CO_2 and H_2O was electrochemically reduced into H_2 and CO in a PV-powered electrolyser at a current density of 50 mA cm^{-2}. The abiotically generated syngas was then fed into a microbial fermenter where a mixed culture of *Clostridium autoethanogenum* and *Clostridium kluyveri* worked together to produce butanol and hexanol at an energetic efficiency of 78% and an overall Faraday efficiency of $\sim$100%.[212] As such, the highest attainable solar-to-chemical efficiency of the integrated system could be projected at 15%, assuming that the existing PV modules deliver a routine energy conversion efficiency of 20%.[212]

5 Future perspectives

Semi-artificial photosynthesis opens a wide spectrum for new solar-to-chemical conversion designs by rationally integrating biocatalysts in the form of proteins and whole cells with synthetic components, which traverses the fields of enzymology, microbiology, materials science, electrochemistry, and photocatalysis. The ultimate goal is to catalyse the transformation of H_2O, CO_2, and N_2 into fuels, chemicals and fertilisers *via* a sustainable path and synthesise value-added fine chemicals with high yield and selectivity with renewable energy sources. Here we briefly propose several promising opportunities for the future development.

At the biotic side, more enzymes or bacteria relevant to fuel/chemical production can be added into the inventory. The methodologies established with model biocatalysts on bespoke electrodes and semiconductor particles can be extrapolated to new biocatalysts to create new reaction pathways. For example, **RuP**–TiO_2 particles were used in early work to adsorb H_2ases for photocatalytic HER.[145] The use of the same light absorber was later extended to CODH, FDH and FccA.[186,193,202] CdS nanorods developed for CdS–H_2ase complexes have been employed to drive N_2-to-NH_3 conversion with N_2ases.[149,200] Likewise, CdS nanoparticles have been *in situ* deposited on the surface of *E. coli* and *M. thermoacetica*.[222,226] It is reasonable to envision that a similar strategy can be applied to other acetogens such as *S. ovata* and methanogens like *M. barkeri*.

Biocatalysts are widely-appreciated for their high product selectivity, yet such catalytic prowess is confined to naturally-occurring reactions. One way to expand the reaction scope is orchestrating various catalysts, including biotic and synthetic, to drive cascade reactions towards more complex and valuable products.[270] For example, an enzyme cascade has been introduced

into a tandem PEC cell to reduce CO_2 into methanol.[198] More opportunities are emerging in this respect to judiciously construct reaction pathways and sensibly direct electron and carbon flux towards desired products.

The second approach arises when advancing genetic techniques meet with enzymology and microbiology. With the derived methodologies, enzymes can be engineered with improved promiscuity and stability. PSII has been introduced with a polyhistidine tag near the stromal side in order to enhance the linkage with Ni-terminated moieties on an electrode surface.[108] Such modifications and single site mutations more broadly are available for other enzymes to improve the interaction with light-absorbing materials. Pathways in microorganisms can be altered to maximise the chemical production or heterologously introduced to unlock unnatural reactions. Metabolic engineering can allow heterotrophic *E. coli* to synthesise sugar from CO_2,[271] and cyanobacteria to drive the reduction of C=C bonds,[272] or produce valuable aromatic compounds directly from CO_2.[273] Engineered microbes with additional pathways can work with light absorbers to yield synthetically useful products beyond their natural metabolites.[238]

Moreover, the genetic toolkit can alter the existing or enable new physiological functionalities in model microorganisms. For example, current production of electrogenic microorganisms can be enhanced by increasing metabolic fluxes, promoting electron shuttle secretion, encouraging biofilm formation, *etc.*[274] Heterologous electron conduits have been transplanted into *E. coli* to confer extracellular electron transfer capability.[274,275] *S. oneidensis* has been engineered to metabolise glucose as carbon and energy source.[276] Beyond this, these techniques also provide powerful means to generate insights into the poorly understood questions with regard to microbial metabolism strategies and electron uptake pathways, which, in turn, will facilitate the rational design of next-generation biohybrid systems.

In parallel, progress at the artificial side can be translated into strengths to stimulate the advancement of semi-artificial photosynthesis systems. Developments in materials science and synthetic chemistry will provide more opportunities in tuning a material's composition, morphology and property at various levels to improve the interaction with biocatalysts or adapt to different reaction conditions. A recent report demonstrated the application of a metal–organic framework to confine FDH within its precisely defined volume and porosity to stabilise enzymatic activity at non-physiological conditions.[277] A metal–organic framework was also employed to encapsulate anaerobic bacteria (*M. thermoacetica*) to protect them against oxidative stress arising from irradiation.[215] Such a strategy is feasibly applicable to other enzymes and bacteria. Another emerging possibility is to foster interaction with biocatalysts at a sub-entity level, instead of forming heterogeneous bio-interfaces. This has been realised by fusing dye molecules with cyt P450 to replace native redox partners,[208] or anchoring Pt nanoparticles with PSI for light-driven H_2 evolution.[278] At a subcellular scale, Au nanoclusters or molecular dyes have been exploited to intervene pathways within cells with light irradiation as bioorthogonal opportunities for intracellular modulation.[231,236,279] Furthermore, the intracellular metabolism can be coupled with extracellular redox transformations to manufacture functional materials such as polymers and inorganic particles.[280–282] These materials may provide additional benefits to promote extracellular electron transfer or cytoprotection.[281]

Advanced photochemistry provides another thrust in future development. Many photosynthetic biohybrid systems are limited by light absorbers that display non-ideal absorption and driving force to perform reactions, or suffer from degradation faster than the inactivation of biocatalysts. Potential solutions may arise from the iterative cycle of design, synthesis and characterisation in the field of artificial photosynthesis, which yields a variety of photocatalysts with fine-tuned properties and morphologies. Progress in this field can instantly contribute to the construction and optimisation of biohybrid systems. For example, carbon nitride and carbon dots emerged as an attractive visible-light absorber due to their well-fit band structure, low cost, and robustness.[66,283] Carbon nitride–H_2ase and carbon dot–H_2ase complexes have been shown effective in photocatalytic H_2 production.[152–154] As such, more applications can be anticipated by replacing H_2ase with other enzymes, or substituting the toxic CdS to interface with acetogenic bacteria. Studies into these newly-derived systems will gain more knowledge of the biotic–abiotic interplay and generate guidelines for the assembly of better systems.

Finally, semi-artificial photosynthesis, in a broader context, also enables a suite of powerful analytical techniques to delve into fundamental questions relevant to physiological functionality, biocatalytic redox chemistry and biotic–abiotic interaction (Fig. 11).[284]

Wiring enzymes or cells to an electrode allows electrochemical methods to probe their redox chemistry and physiological functionality under turnover and non-turnover conditions, through efficient interfacial electron transfer (Fig. 11a).[59,82,285,286] The simplicity of the electrochemical apparatus (typically in a three-electrode electrochemical cell) renders it readily compatible with an extra light source to investigate the light-driven redox reactions of photoactive enzymes (Fig. 11b).[90] Besides stationary electrodes, rotating electrodes, namely rotating disk electrodes or rotating ring disk electrodes, provide an effective way to eliminate the limitations in mass transport that often obscures catalytic features.[287] The rotating ring disk electrode, with an additional ring working electrode surrounding the central disk, enables quantification of reaction products formed at the disk electrode (Fig. 11c).[118]

Complementary to electrochemical methods are spectroscopic techniques, which allow for *in situ* detection of electronic and vibrational changes with relevance to enzymatic or cellular functionalities under electrochemical control and provide structural or mechanistic insights that were otherwise intractable with electrochemistry alone. For instance, ATR-IR was previously deployed to track molecular catalysts and reaction intermediates during catalytic cycles,[288] while it also assisted to probe the enzyme–electrode interaction in H_2ase–TiO_2, FDH–TiO_2 and PSII–ITO systems (Fig. 11d).[102,166,193] Their versatility renders these tools readily transferable to biohybrid assemblies, and offers a high degree of flexibility to work together with (photo)-electrochemistry in *operando* studies (Fig. 11e).

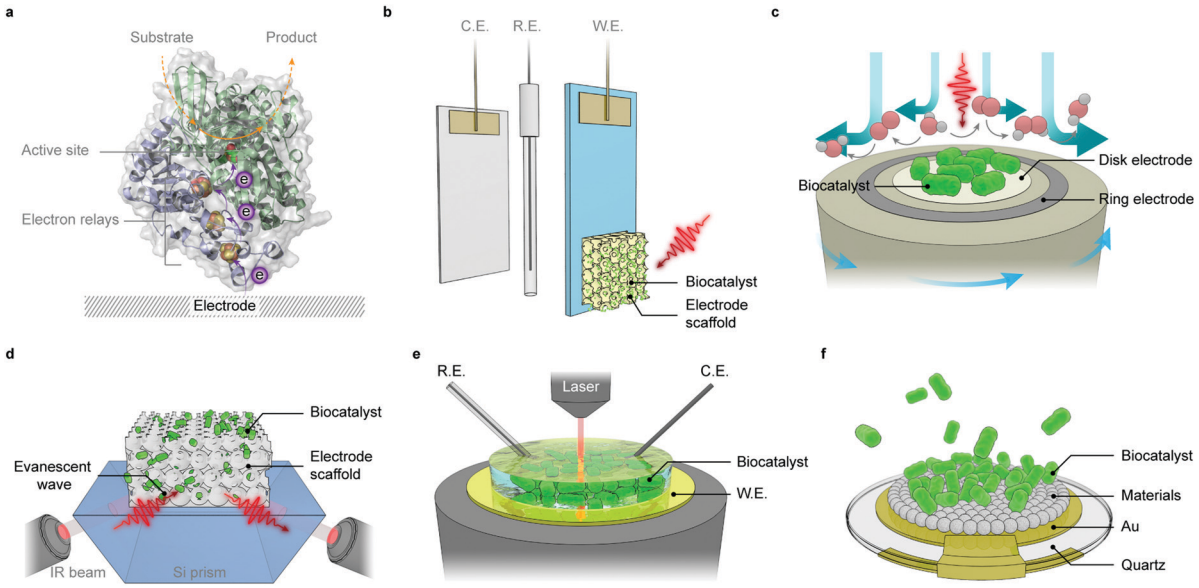

Fig. 11 Analytical techniques employed in semi-artificial photosynthesis.[284] (a) An enzyme–electrode interface. Electrons from the electrode are delivered to the active site *via* intraprotein electron relays. (b) A three-electrode setup comprising a working electrode (W.E.), counter electrode (C.E.) and reference electrode (R.E.) for protein film (photo)electrochemistry and microbial biofilm (photo)electrochemistry. (c) A rotating ring disk electrode with a biocatalyst-adsorbed disk electrode and a Pt ring electrode. The rotation of the apparatus generates a convective flow that hydrodynamically carries reaction products from the disk to the ring electrode for product analysis. (d) An ATR-IR setup with an electrode scaffold deposited on an optical waveguide crystal (*e.g.*, a Si prism). The internal reflection generates an evanescent wave that penetrates into the electrode scaffold by typically ~500 nm. (e) *In situ* spectroelectrochemistry that combines vibrational/electronic spectroscopy with biofilm electrochemistry. Spectroscopic signatures with mechanistic significance can be captured during the course of redox variation with accurate electrochemical control. (f) A typical piezoelectric chip (electrode materials deposited on a Au substrate) for quartz crystal microbalance analysis. Through the mass-frequency relationship, the mass variation stemming from the biocatalyst binding or desorption can be monitored, enabling quantitative insights into bio-electrode interaction and biocatalyst loading capacity.

Time-resolved pump–probe spectroscopy, namely transient absorption spectroscopy, is universally applied in artificial photosynthesis systems to look into kinetic aspects of charge separation and transfer, which take place on a timescale (10^{-12}–10^{-3} s) intractable by other methods.[289] With such temporal resolution, electron transfer at a semiconductor–enzyme interface and the ensuing catalytic turnover can be deconvoluted, enabling unique strength in unravelling kinetic intricacies in photosynthetic biohybrid systems. This technique has been exploited to track the charge transfer in CdS nanorod–H_2ase hybrids and revealed that photogenerated electrons transferred from CdS to the distal relay centre in H_2ase at a rate comparable to that of their relaxation process.[150] In a more complex microbial hybrid system (CdS-sensitised *M. thermoacetica*), transient absorption spectroscopic analysis provided kinetic insights into the electrical interplay between photoexcited semiconductors and acetogenic bacteria, and contributed to the elucidation of pathways connecting extracellular photochemistry and intracellular metabolism.[228]

Beyond electrochemistry and spectroscopy, quartz crystal microbalance (with dissipation) enables a sensitive method to measure the mass change on a piezoelectric quartz chip (Fig. 11f).[76] This allows quantification of enzyme loadings in an electrode scaffold, which is not easily accessible by electrochemical or spectroscopic means and can be further extrapolated to evaluate the nature of enzyme interaction with electrode materials.[166,193] More tools are continuously being added into the toolbox. Recently, electron paramagnetic resonance spectroscopy has been combined with protein film electrochemistry to study metalloenzymes (Cu–Zn superoxide dismutase) adsorbed on a mesoporous ITO electrode under precise potential control.[290] Nanoscale secondary ion mass spectrometry was applied to study the metabolic activity of *G. sulfurreducens* biofilms.[291] These emerging analytic techniques can provide fresh insights from different perspectives to produce a more comprehensive picture of biohybrid systems.

Semi-artificial photosynthesis synergises functional components from different disciplines. Advances in each field will yield new opportunities to further the development and implementation of biohybrid systems. Conclusions drawn from these studies will deepen the current understanding of the biology-materials interplay and form concrete steps to expedite the evolution of semi-artificial photosynthesis towards maturity.

Conflicts of interest

There are no conflicts to declare.

Acknowledgements

This work was supported by a CSC-Cambridge PhD scholarship (to X. F.), a Marie Sklodowska-Curie fellowship (EMES, 744317

to S. K.), and an ERC Consolidator Grant "MatEnSAP" (682833 to E. R.). The authors thank Dr Annika Eisenschmidt, Ms Esther Edwardes Moore, Prof. Julea Butt and Prof. Michael de Volder for the helpful feedback.

References

1 P. K. Nayak, S. Mahesh, H. J. Snaith and D. Cahen, *Nat. Rev. Mater.*, 2019, **4**, 269–285.
2 A. Polman, M. Knight, E. C. Garnett, B. Ehrler and W. C. Sinke, *Science*, 2016, **352**, aad4424.
3 Y. Tachibana, L. Vayssieres and J. R. Durrant, *Nat. Photonics*, 2012, **6**, 511–518.
4 J. H. Montoya, L. C. Seitz, P. Chakthranont, A. Vojvodic, T. F. Jaramillo and J. K. Nørskov, *Nat. Mater.*, 2017, **16**, 70–81.
5 N. Nelson and A. Ben-Shem, *Nat. Rev. Mol. Cell Biol.*, 2004, **5**, 971–982.
6 R. E. Blankenship, *Molecular Mechanisms of Photosynthesis*, Wiley-Blackwell, 2nd edn, 2014.
7 G. G. B. Tcherkez, G. D. Farquhar and T. J. Andrews, *Proc. Natl. Acad. Sci. U. S. A.*, 2006, **103**, 7246–7251.
8 T. J. Erb and J. Zarzycki, *Curr. Opin. Biotechnol.*, 2018, **49**, 100–107.
9 M. Hagemann and H. Bauwe, *Curr. Opin. Chem. Biol.*, 2016, **35**, 109–116.
10 X.-G. Zhu, S. P. Long and D. R. Ort, *Annu. Rev. Plant Biol.*, 2010, **61**, 235–261.
11 R. E. Blankenship, D. M. Tiede, J. Barber, G. W. Brudvig, G. Fleming, M. Ghirardi, M. R. Gunner, W. Junge, D. M. Kramer, A. Melis, T. A. Moore, C. C. Moser, D. G. Nocera, A. J. Nozik, D. R. Ort, W. W. Parson, R. C. Prince and R. T. Sayre, *Science*, 2011, **332**, 805–809.
12 X.-G. Zhu, S. P. Long and D. R. Ort, *Curr. Opin. Biotechnol.*, 2008, **19**, 153–159.
13 R. Croce and H. van Amerongen, *Nat. Chem. Biol.*, 2014, **10**, 492–501.
14 D. J. Lea-Smith, P. Bombelli, R. Vasudevan and C. J. Howe, *Biochim. Biophys. Acta, Bioenerg.*, 2016, **1857**, 247–255.
15 S. Rumpel, J. F. Siebel, C. Farès, J. Duan, E. Reijerse, T. Happe, W. Lubitz and M. Winkler, *Energy Environ. Sci.*, 2014, **7**, 3296–3301.
16 S. I. Allakhverdiev, V. Thavasi, V. D. Kreslavski, S. K. Zharmukhamedov, V. V. Klimov, S. Ramakrishna, D. A. Los, M. Mimuro, H. Nishihara and R. Carpentier, *J. Photochem. Photobiol., C*, 2010, **11**, 101–113.
17 J. Benemann, *Nat. Biotechnol.*, 1996, **14**, 1101–1103.
18 C. E. Lubner, A. M. Applegate, P. Knörzer, A. Ganago, D. A. Bryant, T. Happe and J. H. Golbeck, *Proc. Natl. Acad. Sci. U. S. A.*, 2011, **108**, 20988–20991.
19 H. Bothe, O. Schmitz, M. G. Yates and W. E. Newton, *Microbiol. Mol. Biol. Rev.*, 2010, **74**, 529–551.
20 A. M. Muro-Pastor and W. R. Hess, *Trends Microbiol.*, 2012, **20**, 548–557.
21 P. Fay, *Microbiol. Rev.*, 1992, **56**, 340–373.
22 S. Chen, T. Takata and K. Domen, *Nat. Rev. Mater.*, 2017, **2**, 17050.
23 Q. Wang and K. Domen, *Chem. Rev.*, 2020, **120**, 919–985.
24 D. Kim, K. K. Sakimoto, D. Hong and P. Yang, *Angew. Chem., Int. Ed.*, 2015, **54**, 3259–3266.
25 J. K. Hurst, *Science*, 2010, **328**, 315.
26 M. G. Walter, E. L. Warren, J. R. McKone, S. W. Boettcher, Q. Mi, E. A. Santori and N. S. Lewis, *Chem. Rev.*, 2010, **110**, 6446–6473.
27 S. Chen and L.-W. Wang, *Chem. Mater.*, 2012, **24**, 3659–3666.
28 Q. Wang, T. Hisatomi, Q. Jia, H. Tokudome, M. Zhong, C. Wang, Z. Pan, T. Takata, M. Nakabayashi, N. Shibata, Y. Li, I. D. Sharp, A. Kudo, T. Yamada and K. Domen, *Nat. Mater.*, 2016, **15**, 611–615.
29 R. Kobayashi, T. Takashima, S. Tanigawa, S. Takeuchi, B. Ohtani and H. Irie, *Phys. Chem. Chem. Phys.*, 2016, **18**, 27754–27760.
30 K. Maeda, M. Higashi, D. Lu, R. Abe and K. Domen, *J. Am. Chem. Soc.*, 2010, **132**, 5858–5868.
31 A. Iwase, Y. H. Ng, Y. Ishiguro, A. Kudo and R. Amal, *J. Am. Chem. Soc.*, 2011, **133**, 11054–11057.
32 Y. Sasaki, H. Kato and A. Kudo, *J. Am. Chem. Soc.*, 2013, **135**, 5441–5449.
33 S. Keene, R. Bala Chandran and S. Ardo, *Energy Environ. Sci.*, 2019, **12**, 261–272.
34 D. M. Fabian, S. Hu, N. Singh, F. A. Houle, T. Hisatomi, K. Domen, F. E. Osterloh and S. Ardo, *Energy Environ. Sci.*, 2015, **8**, 2825–2850.
35 K. Sivula and R. van de Krol, *Nat. Rev. Mater.*, 2016, **1**, 15010.
36 J. Luo, J.-H. Im, M. T. Mayer, M. Schreier, M. K. Nazeeruddin, N.-G. Park, S. D. Tilley, H. J. Fan and M. Grätzel, *Science*, 2014, **345**, 1593–1596.
37 C. R. Cox, J. Z. Lee, D. G. Nocera and T. Buonassisi, *Proc. Natl. Acad. Sci. U. S. A.*, 2014, **111**, 14057–14061.
38 E. Pastor, F. Le Formal, M. T. Mayer, S. D. Tilley, L. Francàs, C. A. Mesa, M. Grätzel and J. R. Durrant, *Nat. Commun.*, 2017, **8**, 14280.
39 O. Zandi and T. W. Hamann, *Nat. Chem.*, 2016, **8**, 778–783.
40 K. J. Lee, N. Elgrishi, B. Kandemir and J. L. Dempsey, *Nat. Rev. Chem.*, 2017, **1**, 0039.
41 A. Landman, H. Dotan, G. E. Shter, M. Wullenkord, A. Houaijia, A. Maljusch, G. S. Grader and A. Rothschild, *Nat. Mater.*, 2017, **16**, 646–651.
42 A. Vilanova, T. Lopes, C. Spenke, M. Wullenkord and A. Mendes, *Energy Storage Mater.*, 2018, **13**, 175–188.
43 M. R. Singh, K. Papadantonakis, C. Xiang and N. S. Lewis, *Energy Environ. Sci.*, 2015, **8**, 2760–2767.
44 J. Jin, K. Walczak, M. R. Singh, C. Karp, N. S. Lewis and C. Xiang, *Energy Environ. Sci.*, 2014, **7**, 3371–3380.
45 A. D. Handoko, F. Wei, Jenndy, B. S. Yeo and Z. W. Seh, *Nat. Catal.*, 2018, **1**, 922–934.
46 A. M. Appel, J. E. Bercaw, A. B. Bocarsly, H. Dobbek, D. L. DuBois, M. Dupuis, J. G. Ferry, E. Fujita, R. Hille, P. J. A. Kenis, C. A. Kerfeld, R. H. Morris, C. H. F. Peden,

A. R. Portis, S. W. Ragsdale, T. B. Rauchfuss, J. N. H. Reek, L. C. Seefeldt, R. K. Thauer and G. L. Waldrop, *Chem. Rev.*, 2013, **113**, 6621–6658.
47 X. Li, J. Wen, J. Low, Y. Fang and J. Yu, *Sci. China Mater.*, 2014, **57**, 70–100.
48 X. Chang, T. Wang and J. Gong, *Energy Environ. Sci.*, 2016, **9**, 2177–2196.
49 R. Kortlever, J. Shen, K. J. P. Schouten, F. Calle-Vallejo and M. T. M. Koper, *J. Phys. Chem. Lett.*, 2015, **6**, 4073–4082.
50 X. Li, J. Yu, M. Jaroniec and X. Chen, *Chem. Rev.*, 2019, **119**, 3962–4179.
51 S. L. Foster, S. I. P. Bakovic, R. D. Duda, S. Maheshwari, R. D. Milton, S. D. Minteer, M. J. Janik, J. N. Renner and L. F. Greenlee, *Nat. Catal.*, 2018, **1**, 490–500.
52 J. G. Chen, R. M. Crooks, L. C. Seefeldt, K. L. Bren, R. M. Bullock, M. Y. Darensbourg, P. L. Holland, B. Hoffman, M. J. Janik, A. K. Jones, M. G. Kanatzidis, P. King, K. M. Lancaster, S. V. Lymar, P. Pfromm, W. F. Schneider and R. R. Schrock, *Science*, 2018, **360**, eaar6611.
53 A. Banerjee, B. D. Yuhas, E. A. Margulies, Y. Zhang, Y. Shim, M. R. Wasielewski and M. G. Kanatzidis, *J. Am. Chem. Soc.*, 2015, **137**, 2030–2034.
54 J. Liu, M. S. Kelley, W. Wu, A. Banerjee, A. P. Douvalis, J. Wu, Y. Zhang, G. C. Schatz and M. G. Kanatzidis, *Proc. Natl. Acad. Sci. U. S. A.*, 2016, **113**, 5530–5535.
55 H. Hirakawa, M. Hashimoto, Y. Shiraishi and T. Hirai, *J. Am. Chem. Soc.*, 2017, **139**, 10929–10936.
56 A. J. Medford and M. C. Hatzell, *ACS Catal.*, 2017, **7**, 2624–2643.
57 C. J. M. van der Ham, M. T. M. Koper and D. G. H. Hetterscheid, *Chem. Soc. Rev.*, 2014, **43**, 5183–5191.
58 S. Z. Andersen, V. Čolić, S. Yang, J. A. Schwalbe, A. C. Nielander, J. M. McEnaney, K. Enemark-Rasmussen, J. G. Baker, A. R. Singh, B. A. Rohr, M. J. Statt, S. J. Blair, S. Mezzavilla, J. Kibsgaard, P. C. K. Vesborg, M. Cargnello, S. F. Bent, T. F. Jaramillo, I. E. L. Stephens, J. K. Nørskov and I. Chorkendorff, *Nature*, 2019, **570**, 504–508.
59 F. A. Armstrong and J. Hirst, *Proc. Natl. Acad. Sci. U. S. A.*, 2011, **108**, 14049–14054.
60 C. Wombwell and E. Reisner, *Chem. – Eur. J.*, 2015, **21**, 8096–8104.
61 C. Zhang, C. Chen, H. Dong, J.-R. Shen, H. Dau and J. Zhao, *Science*, 2015, **348**, 690–693.
62 D. Brazzolotto, M. Gennari, N. Queyriaux, T. R. Simmons, J. Pécaut, S. Demeshko, F. Meyer, M. Orio, V. Artero and C. Duboc, *Nat. Chem.*, 2016, **8**, 1054–1060.
63 J. W. Lee, D. Na, J. M. Park, J. Lee, S. Choi and S. Y. Lee, *Nat. Chem. Biol.*, 2012, **8**, 536–546.
64 J. Nielsen and Jay D. Keasling, *Cell*, 2016, **164**, 1185–1197.
65 H. Kasap, D. S. Achilleos, A. Huang and E. Reisner, *J. Am. Chem. Soc.*, 2018, **140**, 11604–11607.
66 H. Kasap, C. A. Caputo, B. C. M. Martindale, R. Godin, V. W.-h. Lau, B. V. Lotsch, J. R. Durrant and E. Reisner, *J. Am. Chem. Soc.*, 2016, **138**, 9183–9192.
67 D. W. Wakerley, M. F. Kuehnel, K. L. Orchard, K. H. Ly, T. E. Rosser and E. Reisner, *Nat. Energy*, 2017, **2**, 17021.
68 T. Uekert, M. F. Kuehnel, D. W. Wakerley and E. Reisner, *Energy Environ. Sci.*, 2018, **11**, 2853–2857.
69 T. Uekert, H. Kasap and E. Reisner, *J. Am. Chem. Soc.*, 2019, **141**, 15201–15210.
70 K. E. Dalle, J. Warnan, J. J. Leung, B. Reuillard, I. S. Karmel and E. Reisner, *Chem. Rev.*, 2019, **119**, 2752–2875.
71 N. Cox, M. Retegan, F. Neese, D. A. Pantazis, A. Boussac and W. Lubitz, *Science*, 2014, **345**, 804–808.
72 J. Jia, L. C. Seitz, J. D. Benck, Y. Huo, Y. Chen, J. W. D. Ng, T. Bilir, J. S. Harris and T. F. Jaramillo, *Nat. Commun.*, 2016, **7**, 13237.
73 X. Zhou, R. Liu, K. Sun, Y. Chen, E. Verlage, S. A. Francis, N. S. Lewis and C. Xiang, *ACS Energy Lett.*, 2016, **1**, 764–770.
74 L. Buzzetti, G. E. M. Crisenza and P. Melchiorre, *Angew. Chem., Int. Ed.*, 2019, **58**, 3730–3747.
75 N. Heidary, K. H. Ly and N. Kornienko, *Nano Lett.*, 2019, **19**, 4817–4826.
76 N. Kornienko, N. Heidary, G. Cibin and E. Reisner, *Chem. Sci.*, 2018, **9**, 5322–5333.
77 N. Kornienko, J. Z. Zhang, K. K. Sakimoto, P. Yang and E. Reisner, *Nat. Nanotechnol.*, 2018, **13**, 890–899.
78 Y. Chen, P. Li, J. Zhou, C. T. Buru, L. Đorđević, P. Li, X. Zhang, M. M. Cetin, J. F. Stoddart, S. I. Stupp, M. R. Wasielewski and O. K. Farha, *J. Am. Chem. Soc.*, 2020, **142**, 1768–1773.
79 N. Plumeré, O. Rüdiger, A. A. Oughli, R. Williams, J. Vivekananthan, S. Pöller, W. Schuhmann and W. Lubitz, *Nat. Chem.*, 2014, **6**, 822–827.
80 H. Li, D. Buesen, S. Dementin, C. Léger, V. Fourmond and N. Plumeré, *J. Am. Chem. Soc.*, 2019, **141**, 16734–16742.
81 A. Heller, *Acc. Chem. Res.*, 1990, **23**, 128–134.
82 C. Léger, S. J. Elliott, K. R. Hoke, L. J. C. Jeuken, A. K. Jones and F. A. Armstrong, *Biochemistry*, 2003, **42**, 8653–8662.
83 M. Can, F. A. Armstrong and S. W. Ragsdale, *Chem. Rev.*, 2014, **114**, 4149–4174.
84 W. Lubitz, H. Ogata, O. Rüdiger and E. Reijerse, *Chem. Rev.*, 2014, **114**, 4081–4148.
85 B. Mondal, J. Song, F. Neese and S. Ye, *Curr. Opin. Chem. Biol.*, 2015, **25**, 103–109.
86 B. M. Hoffman, D. Lukoyanov, Z.-Y. Yang, D. R. Dean and L. C. Seefeldt, *Chem. Rev.*, 2014, **114**, 4041–4062.
87 W. J. Albery and J. R. Knowles, *Biochemistry*, 1976, **15**, 5631–5640.
88 A. Warshel, *Proc. Natl. Acad. Sci. U. S. A.*, 1978, **75**, 5250–5254.
89 W. Lubitz, M. Chrysina and N. Cox, *Photosynth. Res.*, 2019, **142**, 105–125.
90 M. Kato, J. Z. Zhang, N. Paul and E. Reisner, *Chem. Soc. Rev.*, 2014, **43**, 6485–6497.
91 T. Cardona, A. Sedoud, N. Cox and A. W. Rutherford, *Biochim. Biophys. Acta, Bioenerg.*, 2012, **1817**, 26–43.
92 S. De Causmaecker, J. S. Douglass, A. Fantuzzi, W. Nitschke and A. W. Rutherford, *Proc. Natl. Acad. Sci. U. S. A.*, 2019, **116**, 19458–19463.
93 J. Barber, *Chem. Soc. Rev.*, 2009, **38**, 185–196.
94 M. M. Najafpour, T. Ehrenberg, M. Wiechen and P. Kurz, *Angew. Chem., Int. Ed.*, 2010, **49**, 2233–2237.

95 S. Ye, C. Ding, R. Chen, F. Fan, P. Fu, H. Yin, X. Wang, Z. Wang, P. Du and C. Li, *J. Am. Chem. Soc.*, 2018, **140**, 3250–3256.
96 D. Wang, R. N. Sampaio, L. Troian-Gautier, S. L. Marquard, B. H. Farnum, B. D. Sherman, M. V. Sheridan, C. J. Dares, G. J. Meyer and T. J. Meyer, *J. Am. Chem. Soc.*, 2019, **141**, 7926–7933.
97 M. Suga, F. Akita, K. Hirata, G. Ueno, H. Murakami, Y. Nakajima, T. Shimizu, K. Yamashita, M. Yamamoto, H. Ago and J.-R. Shen, *Nature*, 2015, **517**, 99–103.
98 X. Wei, X. Su, P. Cao, X. Liu, W. Chang, M. Li, X. Zhang and Z. Liu, *Nature*, 2016, **534**, 69–74.
99 J. Kern, R. Chatterjee, I. D. Young, F. D. Fuller, L. Lassalle, M. Ibrahim, S. Gul, T. Fransson, A. S. Brewster, R. Alonso-Mori, R. Hussein, M. Zhang, L. Douthit, C. de Lichtenberg, M. H. Cheah, D. Shevela, J. Wersig, I. Seuffert, D. Sokaras, E. Pastor, C. Weninger, T. Kroll, R. G. Sierra, P. Aller, A. Butryn, A. M. Orville, M. Liang, A. Batyuk, J. E. Koglin, S. Carbajo, S. Boutet, N. W. Moriarty, J. M. Holton, H. Dobbek, P. D. Adams, U. Bergmann, N. K. Sauter, A. Zouni, J. Messinger, J. Yano and V. K. Yachandra, *Nature*, 2018, **563**, 421–425.
100 J. Z. Zhang and E. Reisner, *Nat. Rev. Chem.*, 2020, **4**, 6–21.
101 A. Agostiano, A. Ceglie and M. D. Monica, *Bioelectrochem. Bioenerg.*, 1984, **12**, 499–507.
102 X. Fang, K. P. Sokol, N. Heidary, T. A. Kandiel, J. Z. Zhang and E. Reisner, *Nano Lett.*, 2019, **19**, 1844–1850.
103 K. Brinkert, F. Le Formal, X. Li, J. Durrant, A. W. Rutherford and A. Fantuzzi, *Biochim. Biophys. Acta, Bioenerg.*, 2016, **1857**, 1497–1505.
104 M. Kato, T. Cardona, A. W. Rutherford and E. Reisner, *J. Am. Chem. Soc.*, 2012, **134**, 8332–8335.
105 J. Maly, C. Di Meo, M. De Francesco, A. Masci, J. Masojidek, M. Sugiura, A. Volpe and R. Pilloton, *Bioelectrochemistry*, 2004, **63**, 271–275.
106 J. Maly, J. Krejci, M. Ilie, L. Jakubka, J. Masojídek, R. Pilloton, K. Sameh, P. Steffan, Z. Stryhal and M. Sugiura, *Anal. Bioanal. Chem.*, 2005, **381**, 1558–1567.
107 A. Badura, B. Esper, K. Ataka, C. Grunwald, C. Wöll, J. Kuhlmann, J. Heberle and M. Rögner, *Photochem. Photobiol.*, 2006, **82**, 1385–1390.
108 N. Terasaki, M. Iwai, N. Yamamoto, T. Hiraga, S. Yamada and Y. Inoue, *Thin Solid Films*, 2008, **516**, 2553–2557.
109 A. Ruff, *Curr. Opin. Electrochem.*, 2017, **5**, 66–73.
110 A. Badura, D. Guschin, B. Esper, T. Kothe, S. Neugebauer, W. Schuhmann and M. Rögner, *Electroanalysis*, 2008, **20**, 1043–1047.
111 M. Kato, T. Cardona, A. W. Rutherford and E. Reisner, *J. Am. Chem. Soc.*, 2013, **135**, 10610–10613.
112 K. K. Rao, D. O. Hall, N. Vlachopoulos, M. Grätzel, M. C. W. Evans and M. Seibert, *J. Photochem. Photobiol., B*, 1990, **5**, 379–389.
113 W. Wang, Z. Wang, Q. Zhu, G. Han, C. Ding, J. Chen, J.-R. Shen and C. Li, *Chem. Commun.*, 2015, **51**, 16952–16955.
114 J. Li, X. Feng, J. Fei, P. Cai, J. Huang and J. Li, *J. Mater. Chem. A*, 2016, **4**, 12197–12204.
115 J. Li, X. Feng, Y. Jia, Y. Yang, P. Cai, J. Huang and J. Li, *J. Mater. Chem. A*, 2017, **5**, 19826–19835.
116 B. Reuillard, K. H. Ly, P. Hildebrandt, L. J. C. Jeuken, J. N. Butt and E. Reisner, *J. Am. Chem. Soc.*, 2017, **139**, 3324–3327.
117 C.-Y. Lee, B. Reuillard, K. P. Sokol, T. Laftsoglou, C. W. J. Lockwood, S. F. Rowe, E. T. Hwang, J. C. Fontecilla-Camps, L. J. C. Jeuken, J. N. Butt and E. Reisner, *Chem. Commun.*, 2016, **52**, 7390–7393.
118 N. Kornienko, J. Z. Zhang, K. P. Sokol, S. Lamaison, A. Fantuzzi, R. van Grondelle, A. W. Rutherford and E. Reisner, *J. Am. Chem. Soc.*, 2018, **140**, 17923–17931.
119 K. P. Sokol, W. E. Robinson, J. Warnan, N. Kornienko, M. M. Nowaczyk, A. Ruff, J. Z. Zhang and E. Reisner, *Nat. Energy*, 2018, **3**, 944–951.
120 D. Mersch, C.-Y. Lee, J. Z. Zhang, K. Brinkert, J. C. Fontecilla-Camps, A. W. Rutherford and E. Reisner, *J. Am. Chem. Soc.*, 2015, **137**, 8541–8549.
121 K. P. Sokol, D. Mersch, V. Hartmann, J. Z. Zhang, M. M. Nowaczyk, M. Rögner, A. Ruff, W. Schuhmann, N. Plumeré and E. Reisner, *Energy Environ. Sci.*, 2016, **9**, 3698–3709.
122 K. P. Sokol, W. E. Robinson, A. R. Oliveira, J. Warnan, M. M. Nowaczyk, A. Ruff, I. A. C. Pereira and E. Reisner, *J. Am. Chem. Soc.*, 2018, **140**, 16418–16422.
123 K. R. Stieger, S. C. Feifel, H. Lokstein, M. Hejazi, A. Zouni and F. Lisdat, *J. Mater. Chem. A*, 2016, **4**, 17009–17017.
124 D. Ciornii, M. Riedel, K. R. Stieger, S. C. Feifel, M. Hejazi, H. Lokstein, A. Zouni and F. Lisdat, *J. Am. Chem. Soc.*, 2017, **139**, 16478–16481.
125 M. Riedel, W. J. Parak, A. Ruff, W. Schuhmann and F. Lisdat, *ACS Catal.*, 2018, **8**, 5212–5220.
126 M. Riedel, J. Wersig, A. Ruff, W. Schuhmann, A. Zouni and F. Lisdat, *Angew. Chem., Int. Ed.*, 2019, **58**, 801–805.
127 D. Ciornii, A. Kölsch, A. Zouni and F. Lisdat, *Nanoscale*, 2019, **11**, 15862–15870.
128 J. Z. Zhang, P. Bombelli, K. P. Sokol, A. Fantuzzi, A. W. Rutherford, C. J. Howe and E. Reisner, *J. Am. Chem. Soc.*, 2018, **140**, 6–9.
129 T. Wenzel, D. Härtter, P. Bombelli, C. J. Howe and U. Steiner, *Nat. Commun.*, 2018, **9**, 1299.
130 J. Z. Zhang, K. P. Sokol, N. Paul, E. Romero, R. van Grondelle and E. Reisner, *Nat. Chem. Biol.*, 2016, **12**, 1046–1052.
131 M. Pita, D. M. Mate, D. Gonzalez-Perez, S. Shleev, V. M. Fernandez, M. Alcalde and A. L. De Lacey, *J. Am. Chem. Soc.*, 2014, **136**, 5892–5895.
132 C. Tapia, S. Shleev, J. Conesa, A. L. De Lacey and M. Pita, *ACS Catal.*, 2017, **7**, 4881–4889.
133 S. V. Hexter, F. Grey, T. Happe, V. Climent and F. A. Armstrong, *Proc. Natl. Acad. Sci. U. S. A.*, 2012, **109**, 11516–11521.
134 A. K. Jones, E. Sillery, S. P. J. Albracht and F. A. Armstrong, *Chem. Commun.*, 2002, 866–867.
135 K. A. Vincent, A. Parkin and F. A. Armstrong, *Chem. Rev.*, 2007, **107**, 4366–4413.

136 E. Reisner, *Eur. J. Inorg. Chem.*, 2011, 1005–1016.
137 C. C. Page, C. C. Moser, X. Chen and P. L. Dutton, *Nature*, 1999, **402**, 47–52.
138 C. Wombwell, C. A. Caputo and E. Reisner, *Acc. Chem. Res.*, 2015, **48**, 2858–2865.
139 F. A. Armstrong, N. A. Belsey, J. A. Cracknell, G. Goldet, A. Parkin, E. Reisner, K. A. Vincent and A. F. Wait, *Chem. Soc. Rev.*, 2009, **38**, 36–51.
140 A. Parkin, G. Goldet, C. Cavazza, J. C. Fontecilla-Camps and F. A. Armstrong, *J. Am. Chem. Soc.*, 2008, **130**, 13410–13416.
141 M. C. Marques, C. Tapia, O. Gutiérrez-Sanz, A. R. Ramos, K. L. Keller, J. D. Wall, A. L. De Lacey, P. M. Matias and I. A. C. Pereira, *Nat. Chem. Biol.*, 2017, **13**, 544–550.
142 I. Okura, *Coord. Chem. Rev.*, 1985, **68**, 53–99.
143 I. Okura, N. Kaji, S. Aono, T. Kita and A. Yamada, *Inorg. Chem.*, 1985, **24**, 451–453.
144 T. Sakai, D. Mersch and E. Reisner, *Angew. Chem., Int. Ed.*, 2013, **52**, 12313–12316.
145 E. Reisner, D. J. Powell, C. Cavazza, J. C. Fontecilla-Camps and F. A. Armstrong, *J. Am. Chem. Soc.*, 2009, **131**, 18457–18466.
146 E. Reisner, J. C. Fontecilla-Camps and F. A. Armstrong, *Chem. Commun.*, 2009, 550–552.
147 J. Warnan, J. Willkomm, J. N. Ng, R. Godin, S. Prantl, J. R. Durrant and E. Reisner, *Chem. Sci.*, 2017, **8**, 3070–3079.
148 K. A. Brown, S. Dayal, X. Ai, G. Rumbles and P. W. King, *J. Am. Chem. Soc.*, 2010, **132**, 9672–9680.
149 K. A. Brown, M. B. Wilker, M. Boehm, G. Dukovic and P. W. King, *J. Am. Chem. Soc.*, 2012, **134**, 5627–5636.
150 M. B. Wilker, K. E. Shinopoulos, K. A. Brown, D. W. Mulder, P. W. King and G. Dukovic, *J. Am. Chem. Soc.*, 2014, **136**, 4316–4324.
151 K. Wu, H. Zhu, Z. Liu, W. Rodríguez-Córdoba and T. Lian, *J. Am. Chem. Soc.*, 2012, **134**, 10337–10340.
152 C. A. Caputo, M. A. Gross, V. W. Lau, C. Cavazza, B. V. Lotsch and E. Reisner, *Angew. Chem., Int. Ed.*, 2014, **53**, 11538–11542.
153 C. A. Caputo, L. Wang, R. Beranek and E. Reisner, *Chem. Sci.*, 2015, **6**, 5690–5694.
154 G. A. M. Hutton, B. Reuillard, B. C. M. Martindale, C. A. Caputo, C. W. J. Lockwood, J. N. Butt and E. Reisner, *J. Am. Chem. Soc.*, 2016, **138**, 16722–16730.
155 O. Rüdiger, J. M. Abad, E. C. Hatchikian, V. M. Fernandez and A. L. De Lacey, *J. Am. Chem. Soc.*, 2005, **127**, 16008–16009.
156 Y. Park, K. J. McDonald and K.-S. Choi, *Chem. Soc. Rev.*, 2013, **42**, 2321–2337.
157 T. W. Kim and K.-S. Choi, *Science*, 2014, **343**, 990–994.
158 J. D. Benck, B. A. Pinaud, Y. Gorlin and T. F. Jaramillo, *PLoS One*, 2014, **9**, e107942.
159 A. Bachmeier, V. C. C. Wang, T. W. Woolerton, S. Bell, J. C. Fontecilla-Camps, M. Can, S. W. Ragsdale, Y. S. Chaudhary and F. A. Armstrong, *J. Am. Chem. Soc.*, 2013, **135**, 15026–15032.
160 T. E. Rosser and E. Reisner, *ACS Catal.*, 2017, **7**, 3131–3141.
161 N. M. Muresan, J. Willkomm, D. Mersch, Y. Vaynzof and E. Reisner, *Angew. Chem., Int. Ed.*, 2012, **51**, 12749–12753.
162 C.-Y. Lee, H. S. Park, J. C. Fontecilla-Camps and E. Reisner, *Angew. Chem., Int. Ed.*, 2016, **55**, 5971–5974.
163 J. J. Leung, J. Warnan, D. H. Nam, J. Z. Zhang, J. Willkomm and E. Reisner, *Chem. Sci.*, 2017, **8**, 5172–5180.
164 B. Seger, T. Pedersen, A. B. Laursen, P. C. K. Vesborg, O. Hansen and I. Chorkendorff, *J. Am. Chem. Soc.*, 2013, **135**, 1057–1064.
165 F. Lakadamyali and E. Reisner, *Chem. Commun.*, 2011, **47**, 1695–1697.
166 D. H. Nam, J. Z. Zhang, V. Andrei, N. Kornienko, N. Heidary, A. Wagner, K. Nakanishi, K. P. Sokol, B. Slater, I. Zebger, S. Hofmann, J. C. Fontecilla-Camps, C. B. Park and E. Reisner, *Angew. Chem., Int. Ed.*, 2018, **57**, 10595–10599.
167 Y. Zhao, N. C. Anderson, M. W. Ratzloff, D. W. Mulder, K. Zhu, J. A. Turner, N. R. Neale, P. W. King and H. M. Branz, *ACS Appl. Mater. Interfaces*, 2016, **8**, 14481–14487.
168 E. Edwardes Moore, V. Andrei, S. Zacarias, I. A. C. Pereira and E. Reisner, *ACS Energy Lett.*, 2020, **5**, 232–237.
169 C. E. Lubner, R. Grimme, D. A. Bryant and J. H. Golbeck, *Biochemistry*, 2010, **49**, 404–414.
170 H. Krassen, A. Schwarze, B. Friedrich, K. Ataka, O. Lenz and J. Heberle, *ACS Nano*, 2009, **3**, 4055–4061.
171 C. Tapia, R. D. Milton, G. Pankratova, S. D. Minteer, H.-E. Åkerlund, D. Leech, A. L. De Lacey, M. Pita and L. Gorton, *ChemElectroChem*, 2017, **4**, 90–95.
172 C. E. Lubner, P. Knörzer, P. J. N. Silva, K. A. Vincent, T. Happe, D. A. Bryant and J. H. Golbeck, *Biochemistry*, 2010, **49**, 10264–10266.
173 F. Zhao, P. Wang, A. Ruff, V. Hartmann, S. Zacarias, I. A. C. Pereira, M. M. Nowaczyk, M. Rögner, F. Conzuelo and W. Schuhmann, *Energy Environ. Sci.*, 2019, **12**, 3133–3143.
174 P. De Luna, C. Hahn, D. Higgins, S. A. Jaffer, T. F. Jaramillo and E. H. Sargent, *Science*, 2019, **364**, eaav3506.
175 G. Fuchs, *Annu. Rev. Microbiol.*, 2011, **65**, 631–658.
176 S. W. Ragsdale and E. Pierce, *Biochim. Biophys. Acta, Proteins Proteomics*, 2008, **1784**, 1873–1898.
177 K. Schuchmann and V. Müller, *Nat. Rev. Microbiol.*, 2014, **12**, 809–821.
178 C. A. R. Cotton, C. Edlich-Muth and A. Bar-Even, *Curr. Opin. Biotechnol.*, 2018, **49**, 49–56.
179 S. W. Ragsdale, *Crit. Rev. Biochem. Mol. Biol.*, 2004, **39**, 165–195.
180 A. Parkin, J. Seravalli, K. A. Vincent, S. W. Ragsdale and F. A. Armstrong, *J. Am. Chem. Soc.*, 2007, **129**, 10328–10329.
181 J. Fesseler, J.-H. Jeoung and H. Dobbek, *Angew. Chem., Int. Ed.*, 2015, **54**, 8560–8564.
182 M. W. Ribbe, *Angew. Chem., Int. Ed.*, 2015, **54**, 8337–8339.
183 T. Reda, C. M. Plugge, N. J. Abram and J. Hirst, *Proc. Natl. Acad. Sci. U. S. A.*, 2008, **105**, 10654–10658.
184 A. Bassegoda, C. Madden, D. W. Wakerley, E. Reisner and J. Hirst, *J. Am. Chem. Soc.*, 2014, **136**, 15473–15476.

185 W. E. Robinson, A. Bassegoda, E. Reisner and J. Hirst, *J. Am. Chem. Soc.*, 2017, **139**, 9927–9936.
186 T. W. Woolerton, S. Sheard, E. Reisner, E. Pierce, S. W. Ragsdale and F. A. Armstrong, *J. Am. Chem. Soc.*, 2010, **132**, 2132–2133.
187 T. W. Woolerton, S. Sheard, E. Pierce, S. W. Ragsdale and F. A. Armstrong, *Energy Environ. Sci.*, 2011, **4**, 2393–2399.
188 A. Bachmeier, S. Hall, S. W. Ragsdale and F. A. Armstrong, *J. Am. Chem. Soc.*, 2014, **136**, 13518–13521.
189 S. Ikeyama and Y. Amao, *Sustainable Energy Fuels*, 2017, **1**, 1730–1733.
190 Y. Amao, *Sustainable Energy Fuels*, 2018, **2**, 1928–1950.
191 Y. Amao, *Chem. Lett.*, 2017, **46**, 780–788.
192 B. A. Parkinson and P. F. Weaver, *Nature*, 1984, **309**, 148–149.
193 M. Miller, W. E. Robinson, A. R. Oliveira, N. Heidary, N. Kornienko, J. Warnan, I. A. C. Pereira and E. Reisner, *Angew. Chem., Int. Ed.*, 2019, **58**, 4601–4605.
194 S. K. Kuk, Y. Ham, K. Gopinath, P. Boonmongkolras, Y. Lee, Y. W. Lee, S. Kondaveeti, C. Ahn, B. Shin, J.-K. Lee, S. Jeon and C. B. Park, *Adv. Energy Mater.*, 2019, **9**, 1900029.
195 S. Y. Lee, S. Y. Lim, D. Seo, J.-Y. Lee and T. D. Chung, *Adv. Energy Mater.*, 2016, **6**, 1502207.
196 S. K. Kuk, J. Jang, J. Kim, Y. Lee, Y. S. Kim, B. Koo, Y. W. Lee, J. W. Ko, B. Shin, J.-K. Lee and C. B. Park, *ChemSusChem*, 2020, DOI: 10.1002/cssc.202000459.
197 X. Ji, Z. Su, P. Wang, G. Ma and S. Zhang, *Small*, 2016, **12**, 4753–4762.
198 S. K. Kuk, R. K. Singh, D. H. Nam, R. Singh, J.-K. Lee and C. B. Park, *Angew. Chem., Int. Ed.*, 2017, **56**, 3827–3832.
199 S. Zhang, J. Shi, Y. Sun, Y. Wu, Y. Zhang, Z. Cai, Y. Chen, C. You, P. Han and Z. Jiang, *ACS Catal.*, 2019, **9**, 3913–3925.
200 K. A. Brown, D. F. Harris, M. B. Wilker, A. Rasmussen, N. Khadka, H. Hamby, S. Keable, G. Dukovic, J. W. Peters, L. C. Seefeldt and P. W. King, *Science*, 2016, **352**, 448–450.
201 P. Taylor, S. L. Pealing, G. A. Reid, S. K. Chapman and M. D. Walkinshaw, *Nat. Struct. Biol.*, 1999, **6**, 1108–1112.
202 A. Bachmeier, B. J. Murphy and F. A. Armstrong, *J. Am. Chem. Soc.*, 2014, **136**, 12876–12879.
203 M. Mifsud, S. Gargiulo, S. Iborra, I. W. C. E. Arends, F. Hollmann and A. Corma, *Nat. Commun.*, 2014, **5**, 3145.
204 J. Kim, S. H. Lee, F. Tieves, D. S. Choi, F. Hollmann, C. E. Paul and C. B. Park, *Angew. Chem., Int. Ed.*, 2018, **57**, 13825–13828.
205 S. H. Lee, D. S. Choi, M. Pesic, Y. W. Lee, C. E. Paul, F. Hollmann and C. B. Park, *Angew. Chem., Int. Ed.*, 2017, **56**, 8681–8685.
206 H. Hamby, B. Li, K. E. Shinopoulos, H. R. Keller, S. J. Elliott and G. Dukovic, *Proc. Natl. Acad. Sci. U. S. A.*, 2020, **117**, 135–140.
207 J. Wencel-Delord and F. Glorius, *Nat. Chem.*, 2013, **5**, 369–375.
208 N.-H. Tran, D. Nguyen, S. Dwaraknath, S. Mahadevan, G. Chavez, A. Nguyen, T. Dao, S. Mullen, T.-A. Nguyen and L. E. Cheruzel, *J. Am. Chem. Soc.*, 2013, **135**, 14484–14487.
209 C. M. Agapakis, P. M. Boyle and P. A. Silver, *Nat. Chem. Biol.*, 2012, **8**, 527–535.
210 M. J. Smanski, H. Zhou, J. Claesen, B. Shen, M. A. Fischbach and C. A. Voigt, *Nat. Rev. Microbiol.*, 2016, **14**, 135–149.
211 K. K. Sakimoto, N. Kornienko and P. Yang, *Acc. Chem. Res.*, 2017, **50**, 476–481.
212 T. Haas, R. Krause, R. Weber, M. Demler and G. Schmid, *Nat. Catal.*, 2018, **1**, 32–39.
213 S. Cestellos-Blanco, H. Zhang, J. M. Kim, Y.-X. Shen and P. Yang, *Nat. Catal.*, 2020, **3**, 245–255.
214 M. L. Ghirardi, A. Dubini, J. Yu and P.-C. Maness, *Chem. Soc. Rev.*, 2009, **38**, 52–61.
215 Z. Ji, H. Zhang, H. Liu, O. M. Yaghi and P. Yang, *Proc. Natl. Acad. Sci. U. S. A.*, 2018, **115**, 10582–10587.
216 W. Wei, P. Sun, Z. Li, K. Song, W. Su, B. Wang, Y. Liu and J. Zhao, *Sci. Adv.*, 2018, **4**, eaap9253.
217 A. A. Krasnovsky and V. V. Nikandrov, *FEBS Lett.*, 1987, **219**, 93–96.
218 P. Maruthamuthu, S. Muthu, K. Gurunathan, M. Ashokkumar and M. V. C. Sastri, *Int. J. Hydrogen Energy*, 1992, **17**, 863–866.
219 K. Gurunathan, *J. Mol. Catal. A: Chem.*, 2000, **156**, 59–67.
220 S. Pontrelli, T.-Y. Chiu, E. I. Lan, F. Y. H. Chen, P. Chang and J. C. Liao, *Metab. Eng.*, 2018, **50**, 16–46.
221 Y. Honda, H. Hagiwara, S. Ida and T. Ishihara, *Angew. Chem., Int. Ed.*, 2016, **55**, 8045–8048.
222 B. Wang, C. Zeng, K. H. Chu, D. Wu, H. Y. Yip, L. Ye and P. K. Wong, *Adv. Energy Mater.*, 2017, **7**, 1700611.
223 K. P. Kuhl, E. R. Cave, D. N. Abram and T. F. Jaramillo, *Energy Environ. Sci.*, 2012, **5**, 7050–7059.
224 R. K. Thauer, A.-K. Kaster, H. Seedorf, W. Buckel and R. Hedderich, *Nat. Rev. Microbiol.*, 2008, **6**, 579–591.
225 J. Ye, J. Yu, Y. Zhang, M. Chen, X. Liu, S. Zhou and Z. He, *Appl. Catal., B*, 2019, **257**, 117916.
226 K. K. Sakimoto, A. B. Wong and P. Yang, *Science*, 2016, **351**, 74–77.
227 A. W. D. Larkum, *Curr. Opin. Biotechnol.*, 2010, **21**, 271–276.
228 N. Kornienko, K. K. Sakimoto, D. M. Herlihy, S. C. Nguyen, A. P. Alivisatos, C. B. Harris, A. Schwartzberg and P. Yang, *Proc. Natl. Acad. Sci. U. S. A.*, 2016, **113**, 11750–11755.
229 R. Zhang, Y. He, J. Yi, L. Zhang, C. Shen, S. Liu, L. Liu, B. Liu and L. Qiao, *Chem*, 2020, **6**, 234–249.
230 K. K. Sakimoto, S. J. Zhang and P. Yang, *Nano Lett.*, 2016, **16**, 5883–5887.
231 H. Zhang, H. Liu, Z. Tian, D. Lu, Y. Yu, S. Cestellos-Blanco, K. K. Sakimoto and P. Yang, *Nat. Nanotechnol.*, 2018, **13**, 900–905.
232 B. Wang, Z. Jiang, J. C. Yu, J. Wang and P. K. Wong, *Nanoscale*, 2019, **11**, 9296–9301.
233 M. Chen, X.-F. Zhou, Y.-Q. Yu, X. Liu, R. J.-X. Zeng, S.-G. Zhou and Z. He, *Environ. Int.*, 2019, **127**, 353–360.
234 P. Gai, W. Yu, H. Zhao, R. Qi, F. Li, L. Liu, F. Lv and S. Wang, *Angew. Chem., Int. Ed.*, 2020, **59**, 7224–7229.
235 S. F. Rowe, G. Le Gall, E. V. Ainsworth, J. A. Davies, C. W. J. Lockwood, L. Shi, A. Elliston, I. N. Roberts, K. W. Waldron, D. J. Richardson, T. A. Clarke, L. J. C. Jeuken, E. Reisner and J. N. Butt, *ACS Catal.*, 2017, **7**, 7558–7566.

236 J. H. Park, S. H. Lee, G. S. Cha, D. S. Choi, D. H. Nam, J. H. Lee, J.-K. Lee, C.-H. Yun, K. J. Jeong and C. B. Park, *Angew. Chem., Int. Ed.*, 2015, **54**, 969–973.
237 X. Wang, T. Saba, H. H. P. Yiu, R. F. Howe, J. A. Anderson and J. Shi, *Chem*, 2017, **2**, 621–654.
238 J. Guo, M. Suástegui, K. K. Sakimoto, V. M. Moody, G. Xiao, D. G. Nocera and N. S. Joshi, *Science*, 2018, **362**, 813–816.
239 E. M. Nichols, J. J. Gallagher, C. Liu, Y. Su, J. Resasco, Y. Yu, Y. Sun, P. Yang, M. C. Y. Chang and C. J. Chang, *Proc. Natl. Acad. Sci. U. S. A.*, 2015, **112**, 11461–11466.
240 J. P. Torella, C. J. Gagliardi, J. S. Chen, D. K. Bediako, B. Colón, J. C. Way, P. A. Silver and D. G. Nocera, *Proc. Natl. Acad. Sci. U. S. A.*, 2015, **112**, 2337–2342.
241 C. Liu, B. C. Colón, M. Ziesack, P. A. Silver and D. G. Nocera, *Science*, 2016, **352**, 1210–1213.
242 D. K. Dogutan and D. G. Nocera, *Acc. Chem. Res.*, 2019, **52**, 3143–3148.
243 C. Liu, K. K. Sakimoto, B. C. Colón, P. A. Silver and D. G. Nocera, *Proc. Natl. Acad. Sci. U. S. A.*, 2017, **114**, 6450–6455.
244 R. M. Rodrigues, X. Guan, J. A. Iñiguez, D. A. Estabrook, J. O. Chapman, S. Huang, E. M. Sletten and C. Liu, *Nat. Catal.*, 2019, **2**, 407–414.
245 K. Rabaey and R. Rozendal, *Nat. Rev. Microbiol.*, 2010, **8**, 706–716.
246 D. R. Lovley, *Environ. Microbiol. Rep.*, 2011, **3**, 27–35.
247 A. J. McCormick, P. Bombelli, R. W. Bradley, R. Thorne, T. Wenzel and C. J. Howe, *Energy Environ. Sci.*, 2015, **8**, 1092–1109.
248 C. Liu, J. J. Gallagher, K. K. Sakimoto, E. M. Nichols, C. J. Chang, M. C. Y. Chang and P. Yang, *Nano Lett.*, 2015, **15**, 3634–3639.
249 F. Qian, H. Wang, Y. Ling, G. Wang, M. P. Thelen and Y. Li, *Nano Lett.*, 2014, **14**, 3688–3693.
250 Y. Su, S. Cestellos-Blanco, J. M. Kim, Y.-x. Shen, Q. Kong, D. Lu, C. Liu, H. Zhang, Y. Cao and P. Yang, *Joule*, 2020, **4**, 800–811.
251 S. Li, C. Cheng and A. Thomas, *Adv. Mater.*, 2017, **29**, 1602547.
252 K. K. Sakimoto, N. Kornienko, S. Cestellos-Blanco, J. Lim, C. Liu and P. Yang, *J. Am. Chem. Soc.*, 2018, **140**, 1978–1985.
253 V. Flexer and L. Jourdin, *Acc. Chem. Res.*, 2020, **53**, 311–321.
254 K. B. Gregory, D. R. Bond and D. R. Lovley, *Environ. Microbiol.*, 2004, **6**, 596–604.
255 S. M. Strycharz, R. H. Glaven, M. V. Coppi, S. M. Gannon, L. A. Perpetua, A. Liu, K. P. Nevin and D. R. Lovley, *Bioelectrochemistry*, 2011, **80**, 142–150.
256 D. E. Ross, J. M. Flynn, D. B. Baron, J. A. Gralnick and D. R. Bond, *PLoS One*, 2011, **6**, e16649.
257 Y.-C. Yong, Y.-Y. Yu, X. Zhang and H. Song, *Angew. Chem., Int. Ed.*, 2014, **53**, 4480–4483.
258 B. E. Logan and K. Rabaey, *Science*, 2012, **337**, 686–690.
259 K. B. Gregory and D. R. Lovley, *Environ. Sci. Technol.*, 2005, **39**, 8943–8947.
260 S. M. Strycharz, T. L. Woodard, J. P. Johnson, K. P. Nevin, R. A. Sanford, F. E. Löffler and D. R. Lovley, *Appl. Environ. Microbiol.*, 2008, **74**, 5943–5947.
261 S. M. Strycharz, S. M. Gannon, A. R. Boles, A. E. Franks, K. P. Nevin and D. R. Lovley, *Environ. Microbiol. Rep.*, 2010, **2**, 289–294.
262 X. Fang, S. Kalathil, G. Divitini, Q. Wang and E. Reisner, *Proc. Natl. Acad. Sci. U. S. A.*, 2020, **117**, 5074–5080.
263 N. Heidary, N. Kornienko, S. Kalathil, X. Fang, K. H. Ly, H. F. Greer and E. Reisner, *J. Am. Chem. Soc.*, 2020, **142**, 5194–5203.
264 N. J. Claassens, D. Z. Sousa, V. A. P. M. dos Santos, W. M. de Vos and J. van der Oost, *Nat. Rev. Microbiol.*, 2016, **14**, 692–706.
265 J. S. Deutzmann and A. M. Spormann, *ISME J.*, 2016, **11**, 704–714.
266 P. T. Ha, S. R. Lindemann, L. Shi, A. C. Dohnalkova, J. K. Fredrickson, M. T. Madigan and H. Beyenal, *Nat. Commun.*, 2017, **8**, 13924.
267 B. Schiel-Bengelsdorf and P. Dürre, *FEBS Lett.*, 2012, **586**, 2191–2198.
268 C. M. Humphreys and N. P. Minton, *Curr. Opin. Biotechnol.*, 2018, **50**, 174–181.
269 N. J. Claassens, C. A. R. Cotton, D. Kopljar and A. Bar-Even, *Nat. Catal.*, 2019, **2**, 437–447.
270 F. Rudroff, M. D. Mihovilovic, H. Gröger, R. Snajdrova, H. Iding and U. T. Bornscheuer, *Nat. Catal.*, 2018, **1**, 12–22.
271 N. Antonovsky, S. Gleizer, E. Noor, Y. Zohar, E. Herz, U. Barenholz, L. Zelcbuch, S. Amram, A. Wides, N. Tepper, D. Davidi, Y. Bar-On, T. Bareia, D. G. Wernick, I. Shani, S. Malitsky, G. Jona, A. Bar-Even and R. Milo, *Cell*, 2016, **166**, 115–125.
272 K. Köninger, Á. Gómez Baraibar, C. Mügge, C. E. Paul, F. Hollmann, M. M. Nowaczyk and R. Kourist, *Angew. Chem., Int. Ed.*, 2016, **55**, 5582–5585.
273 J. Ni, H.-Y. Liu, F. Tao, Y.-T. Wu and P. Xu, *Angew. Chem., Int. Ed.*, 2018, **57**, 15990–15994.
274 M. A. TerAvest and C. M. Ajo-Franklin, *Biotechnol. Bioeng.*, 2016, **113**, 687–697.
275 M. A. TerAvest, T. J. Zajdel and C. M. Ajo-Franklin, *ChemElectroChem*, 2014, **1**, 1874–1879.
276 D. Choi, S. B. Lee, S. Kim, B. Min, I.-G. Choi and I. S. Chang, *Bioresour. Technol.*, 2014, **154**, 59–66.
277 Y. Chen, P. Li, H. Noh, C.-W. Kung, C. T. Buru, X. Wang, X. Zhang and O. K. Farha, *Angew. Chem., Int. Ed.*, 2019, **58**, 7682–7686.
278 I. J. Iwuchukwu, M. Vaughn, N. Myers, H. O'Neill, P. Frymier and B. D. Bruce, *Nat. Nanotechnol.*, 2009, **5**, 73–79.
279 Y. V. Lee and B. Tian, *Nano Lett.*, 2019, **19**, 2189–2197.
280 G. Fan, C. M. Dundas, A. J. Graham, N. A. Lynd and B. K. Keitz, *Proc. Natl. Acad. Sci. U. S. A.*, 2018, **115**, 4559–4564.
281 T. Song, H. Zhang, H. Liu, D. Zhang, H. Wang, Y. Yang, H. Yuan and J. Xie, *Bioresour. Technol.*, 2017, **243**, 573–582.
282 C. M. Dundas, A. J. Graham, D. K. Romanovicz and B. K. Keitz, *ACS Synth. Biol.*, 2018, **7**, 2726–2736.
283 B. C. M. Martindale, G. A. M. Hutton, C. A. Caputo and E. Reisner, *J. Am. Chem. Soc.*, 2015, **137**, 6018–6025.

284 N. Kornienko, K. H. Ly, W. E. Robinson, N. Heidary, J. Z. Zhang and E. Reisner, *Acc. Chem. Res.*, 2019, **52**, 1439–1448.
285 M. del Barrio, M. Sensi, C. Orain, C. Baffert, S. Dementin, V. Fourmond and C. Léger, *Acc. Chem. Res.*, 2018, **51**, 769–777.
286 E. Marsili, J. B. Rollefson, D. B. Baron, R. M. Hozalski and D. R. Bond, *Appl. Environ. Microbiol.*, 2008, **74**, 7329–7337.
287 T. Reda and J. Hirst, *J. Phys. Chem. B*, 2006, **110**, 1394–1404.
288 B. Reuillard, K. H. Ly, T. E. Rosser, M. F. Kuehnel, I. Zebger and E. Reisner, *J. Am. Chem. Soc.*, 2017, **139**, 14425–14435.
289 J. Willkomm, K. L. Orchard, A. Reynal, E. Pastor, J. R. Durrant and E. Reisner, *Chem. Soc. Rev.*, 2016, **45**, 9–23.
290 K. Abdiaziz, E. Salvadori, K. P. Sokol, E. Reisner and M. M. Roessler, *Chem. Commun.*, 2019, **55**, 8840–8843.
291 G. L. Chadwick, F. Jiménez Otero, J. A. Gralnick, D. R. Bond and V. J. Orphan, *Proc. Natl. Acad. Sci. U. S. A.*, 2019, **116**, 20716–20724.
292 Z. S. Wang, K. Sayama and H. Sugihara, *J. Phys. Chem. B*, 2005, **109**, 22449–22455.
293 R. Beranek, *Adv. Phys. Chem.*, 2011, 786759.
294 J. Zhang, X. Chen, K. Takanabe, K. Maeda, K. Domen, J. D. Epping, X. Fu, M. Antonietti and X. Wang, *Angew. Chem., Int. Ed.*, 2010, **49**, 441–444.
295 B. C. M. Martindale, E. Joliat, C. Bachmann, R. Alberto and E. Reisner, *Angew. Chem., Int. Ed.*, 2016, **55**, 9402–9406.
296 M. F. Kuehnel, K. L. Orchard, K. E. Dalle and E. Reisner, *J. Am. Chem. Soc.*, 2017, **139**, 7217–7223.
297 D. P. Hari and B. König, *Chem. Commun.*, 2014, **50**, 6688–6699.

